A STUDY OF LINEAR AND NONLINEAR REFRACTIVE INDEX CHANGES AND OPTICAL ABSORPTIONS IN QUANTUM DOTS

by

Erem BİRŞEY

The Institute of Graduate Studies in

Science and Engineering

Yeditepe University

2014

T.C.
YEDİTEPE ÜNİVERSİTESİ
FEN BİLİMLERİ ENSTİTÜSÜ

A study of Linear and Nonlinear Refractive Index Changes and absorption Coefficient in quantum dots.
(konu)

ONAY:

Yrd. Doç. Dr. Uldan Üstüğlu Ünal
(danışman) (imza)

Prof. Dr. M Hikmet Yükselici
(üye) (imza)

Doç. Dr. Ertan Akşahin
(üye) (imza)

TESLİM EDEN : Erem BIRŞEY
TEZ SAVUNMA TARİHİ : 08.08.2014
TEZ ONAY TARİHİ :

T.C. Yeditepe Üniversitesi
Fen Bilimleri Enstitü Müdürlüğü

ACKNOWLEDGEMENTS

I would like to express my gratitude to all those who gave me the possibility to complete this graduation project. I am deeply indebted to my supervisor Assist. Prof. Dr. Vildan Üstoğlu Ünal for her patient guidance, valuable suggestions and encouragement during this research work and writing of the graduation project.

Also I want to thank to the Department of Physics in Yeditepe University for their support.

I owe much more than a thank to my family for their encouragement, unlimited love, trust, and endless patient throughout my study.

ABSTRACT

A STUDY OF LINEAR AND NONLINEAR REFRACTIVE INDEX CHANGES AND OPTICAL ABSORPTIONS IN QUANTUM DOTS

Important advances in both epitaxial growth and laser technologies have created a growing interest in the linear and nonlinear optical properties of quantum dots (QDs). In this study, the nonlinear optical properties, including the linear and nonlinear changes in the refractive index and optical absorption, have been studied, with the electric field effect. The electronic structures of the disk-like and spherical QDs are calculated using the effective-mass and dipole approximation, for the two different confining potentials; an infinitely deep and a parabolic. The nonlinear optical coefficients are written within the density matrix formalism. The results show that the total change in the refractive index increases with increasing QD size but the total absorption coefficients decrease. The peaks are blue-shifted for decreasing QD size. The nonlinear optical properties increase as the strength of the applied electric field and the optical intensity increase. Comparison of QD types shows that the refractive index changes and the absorption coefficients in the disk-like QD are lower than those in the spherical QD. Also the infinitely deep confining potential results in higher confinement effects and optical response compared to those observed in the parabolic potential case.

ÖZET

KUANTUM NOKTALARINDAKİ DOĞRUSAL, DOĞRUSAL OLMAYAN KIRILMA ENDEKSİ DEĞİŞİMLERİ VE OPTİK ABSORPSİYON ÇALIŞMASI

Epitaksiyal büyüme ve laser teknolojilerindeki önemli gelişmeler kuantum noktalarının doğrusal ve doğrusal olmayan optik özellikleri üzerinde giderek artan bir ilgi yaratmıştır. Bu çalışmada, doğrusal ve doğrusal olmayan kırılma indisindeki değişmeler ve optik soğurmayı kapsayan doğrusal olmayan optik özellikler, elektrik alan etkisiyle beraber incelenmiştir. İki boyutlu (disk gibi) ve küresel kuantum noktalarının elektronik yapıları, iki farklı hapsedilen potansiyel için (sonsuz derinlikteki potansiyel ve parabolik potansiyel), etkin kütle ve dipol yaklaşımı kullanılarak hesaplanmıştır. Doğrusal olmayan optik katsayılar, yoğunluk matrisi formalizasyonu kullanılarak yazılmıştır. Sonuçlar göstermiştir ki, kırılma indisindeki toplam değişim kuantum noktası büyüdükçe artarken, toplam soğurma katsayısı azalmaktadır. Tepe noktaları, kuantum noktasının boyutunun azalmasıyla mavi ışıma bölgesine kayar. Doğrusal olmayan optik özellikler, uygulanan elektrik alanının gücü ve optik yoğunluk arttıkça artmaktadır. Kuantum noktalarının tiplerinin karşılaştırılmasında ise, iki boyutlu (disk gibi) kuantum noktasındaki kırılma indisi değişimi ve soğurma katsayısının küresel kuantum noktasına göre daha düşük olduğu görülmüştür. Ayrıca, sonsuz derinlikteki potansiyel, parabolik potansiyel durumunda gözlemlenenlere göre, daha yüksek hapsetme etkisi ve optik tepkiyle sonuçlanmaktadır.

TABLE OF CONTENTS

ACKNOWLEDGEMENT.....ii

ABSTRACT.....iii

ÖZET.....iv

TABLE OF CONTENTS.....v

LIST OF FIGURES.....vii

LIST OF TABLES.....xi

LIST OF SYMBOLS /ABBREVIATIONS.....xii

1. INTRODUCTION.....1

2. THEORETICAL FRAMEWORK.....6

2.1. DENSITY MATRIX FORMALISM.....8

2.2. TWO-LEVEL ATOM APPROXIMATION.....11

2.3. EFFECTIVE MASS APPROXIMATION.....12

2.4. STARK EFFECT.....13

3. CALCULATIONS.....15

3.1. DISC-LIKE QD WITH INFINITELY DEEP CONFINING POTENTIAL.. 16

3.1.1. Stark Effect On The Disc-Like QD With Infinitely Deep Confining Potential.....23

3.2. DISC-LIKE QD WITH PARABOLIC CONFINING POTENTIAL 24

3.3. SPHERICAL QD WITH INFINITELY DEEP CONFINING POTENTIAL.27

3.3.1. Stark Effect On The Spherical QD With Infinitely Deep Confining Potential.....32

4. NUMERICAL RESULTS AND DISCUSSION.....34

5. CONCLUSION.....61

REFERENCES.....62

LIST OF FIGURES

Figure 2.1. (a) Schematic plot of the energies for electrons in QDs, (b) near-resonant excitation of the two level system.....11

Figure 2.2. Effective Mass Approxiamtion and envelope wavefunction.....13

Figure 3.1. Diagram for the disc-like QD.....16

Figure 3.2. Bessel's function of the first kind.....19

Figure 3.3. Diagram for the probability densities $|\psi_0|^2$ and $|\psi_1|^2$ of the electron confined in disc-like QD, infinitely deep potential.....21

Figure 3.4. Diagram for the probability densities $|\psi_0|^2$ and $|\psi_1|^2$ of the electron confined in disc-like QD, parabolic potential.....27

Figure 3.5. Diagram for the spherical QD.....28

Figure 3.6. Diagram for the probability densities $|\psi_0|^2$ and $|\psi_1|^2$ of the electron confined in spherical QD, infinitely deep potential.....31

Figure 4.1. The energies of ground and excited states as a function of dot size parameter η for the disc-like, infinitely deep confining potential, no external field.....35

Figure 4.2. The energies of ground and excited states as a function of dot size parameter η for the spherical QD, infinitely deep confining potential, no external field....35

Figure 4.3. Effect of the QD shape on E_{10}, infinitely deep confining potential, no external field.....36

Figure 4.4. E_0 and E_1 as a function of (a) η and (b) ω_0, disc-like QD, parabolic potential, no external field.....37

Figure 4.5. Effect of the confining potential on E_{10}, disc-like QD, no external field 37

Figure 4.6. Effect of the QD shape on $|\mu_{10}|^2$,infinitely deep potential, no external field..40

Figure 4.7. Effect of the confinement potential on the dipole matrix element $|\mu_{10}|^2$, disc-like QD, no external field.....40

Figure 4.8. Effect of the external electric field F on the dipole element $|\mu_{10}|^2$, disc-like QD, infinitely deep potential, $\eta = 8$ 41

Figure 4.9. Variation of the diagonal matrix elements μ'_{00} and μ'_{11} with the size of disc-like QD, infinitely deep potential, $F = 10\ kV/cm$.....42

Figure 4.10. Effect of the external electric field F on the dipole element $|\mu_{10}|^2$, with different disc-like QD sizes, infinitely deep potential, $F = 10kV/cm$.....42

Figure 4.11. Variation of $|(\mu_{11} - \mu_{00})/\mu_{10}|^2$ with the external electric field F, infinitely deep potential, disc-like QD, $\eta = 8$.....43

Figure 4.12. Variation of parabolic and Coulomb potential energies with QD size, disc-like QD, no external field.....44

Figure 4.13. The linear, third-order nonlinear and total RIC as a function of photon energy, $\eta = 8$, $I = 1.0\ MW/cm^2$, disc-like QD, infinitely deep potential, no external field.....45

Figure 4.14. The linear, third-order nonlinear and total RIC as a function of photon energy, for various disc-like QD sizes, $I = 1.0\ MW/cm^2$, infinitely deep potential, no external field.....46

Figure 4.15. Third-order nonlinear RIC as a function of photon energy, for various intensities, $\eta = 8$, disc-like QD, infinitely deep potential, no external field..47

Figure 4.16. Total RIC as a function of photon energy, for various intensities, $\eta = 8$, disc-like QD, infinitely deep potential, no external field.....47

Figure 4.17. The linear, third-order nonlinear and total RIC as a function of photon energy, for various spherical QD sizes, $I = 1.0\ MW/cm^2$, infinitely deep potential, no external field.....48

Figure 4.18. Third-order nonlinear RIC as a function of photon energy for various intensities, $\eta = 8$, spherical QD, infinitely deep potential, no external field..49

Figure 4.19. Total RIC as a function of photon energy for various intensities, $\eta = 8$, spherical QD, infinitely deep potential, no external field.....50

Figure 4.20. Comparison of total RIC of the spherical QD with that of the disc-like dot, infinitely deep potential, no external field, $I = 1.0\ MW/cm^2$ and $\eta = 8$ 51

Figure 4.21. Contribution of the second term in Equation (2.24) to the change in the refractive index as a function of photon energy, for various disc-like QD size, infinitely deep potential, $F = 10\ kV/cm, I = 1.0\ MW/cm^2$ 52

Figure 4.22. Contribution of the second term in Equation (2.24) to the change in the refractive index as a function of photon energy, for various external field strengths, disc-like QD, infinitely deep potential, $\eta = 8,\ I = 1.0\ MW/\ cm^2$ 52

Figure 4.23. The linear, third-order nonlinear and total RIC as a function of photon energy, for various disc-like QD sizes, $I = 1.0\ MW/cm^2$, parabolic potential, no external field.....53

Figure 4.24. Effect of the confining potential on the total RIC in the disc-like QD, $I = 1.0\ MW/cm^2$ and $\eta = 8$, no external field.....54

Figure 4.25. Total RIC as a function of photon energy for various intensities, $\eta = 8$, disc-like QD, parabolic confinement, no external field.....54

Figure 4.26. The linear, third-order nonlinear and total absorption coefficients as a function of photon energy, for various disc-like QD sizes, $I = 1.0\ MW/cm^2$, infinitely deep confining potential, no external field.....56

Figure 4.27. The linear, third-order nonlinear and total absorption coefficients as a function of photon energy, for various spherical QD sizes, $I = 1.0\ MW/cm^2$, infinitely deep confining potential, no external field.....57

Figure 4.28. Effect of the QD shape on the total absorption coefficient $\alpha^{(total)}$, $\eta = 8$, $I = 1.0\ MW/cm^2$, infinitely deep confining potential, no external field.....57

Figure 4.29. Effect of the confining potential on the total absorption coefficient $\alpha^{(total)}$, $\eta = 8$, $I = 1.0\ MW/cm^2$, infinitely deep confining potential, no external field.....58

Figure 4.30. Effect of the intensity of the incoming photons on the total absorption coefficient $\alpha^{(total)}$, $\eta = 8$, disc-like QD, parabolic potential, $I = 1.0\ MW/\ cm^2$ no external field.....59

Figure 4.31. Variation of the maximum absorption coefficient $\alpha^{(max)}$ with the frequency ω_o of the parabolic potential, disc-like QD, parabolic potential, $I = 1.0\ MW/cm^2$, no external field.....60

LIST OF TABLES

Table 4.1. Stark effect, perturbed and unperturbed energy differences E_{10} and E'_{10} for various dot size, infinitely deep potential, disc-like and spherical QD.....38

Table 4.2. Stark effect, perturbed, unperturbed energy differences E_{10} and E'_{10} for various applied electric field, infinitely deep potential, disc-like and spherical QD, $\eta = 8$.....38

Table 4.3. Stark effect, perturbed dipole matrix elements μ'_{00}, μ'_{11} and μ'_{10} for various applied electric fields, infinitely deep potential, disc-like QD.....39

LIST OF SYMBOLS / ABBREVIATIONS

a_o^*	Effective Bohr Radius
a_o	Bohr Radius
a	Radius of quantum dot
c	speed of light in free space
C	Arbitrary constant
$C_n^s(t)$	Probability amplitude
$-e$	Charge of the electron
$E(t)$	Electric field of the incident electromagnetic field
E_{10}	Energy difference between the states 0 and 1
$E_n{}'$	Perturbed energy of the state n
$E_n^{(0)}$	Unperturbed energy of the state n
$\vec{\mu}$	Electric dipole moment
$\vec{F}$	External electric field
H	Hamiltonian

I	Intensity of the incident light
J_m	Bessel function of the first kind, of the order m
J_l	Spherical Bessel function of the order of l
$\vec{k}$	Wavevector
m	order of the Bessel function
m_e	mass of the free electron
m^*	effective mass
N	Free electron density
n_r	Refractive index
N_m	Neumann function of the order of m
$P(t)$	Polarization
$\vec{r}$	Position Vector
P_l^m	Legendre function
RIC	Refractive Index Change
QD	Quantum Dot
ω	Frequency of the incident optical field
ω_0	Frequency of the parabolic confining potential

$\alpha^{(1)}$	Linear absorption coefficient
$\alpha^{(3)}$	Third-order nonlinear absorption coefficient
$\alpha^{(total)}$	Total Absorption Coefficient
ε_0	Permittivity of free space
ϵ	Static dielectric constant
$\hat{\rho}$	Density matrix
h	Planck constant
$\hbar w = h\nu$	incident photon energy
η	Quantum dot size parameter
Γ_0	Relaxation rate
ϕ	Azimuthal Angle
ψ_n	envelope wave function
$\Psi_n(\vec{r})$	Eigensolution of time-independent Schrödinger's equation
$\chi^{(1)}$	Linear optical susceptibility
$\chi^{(2)}$	Second-order nonlinear optical susceptibility
$\chi^{(3)}$	Third-order nonlinear optical susceptibility

$\Delta n^{(1)}$	Linear refractive index change
$\Delta n^{(3)}$	Third-order nonlinear refractive index change
$\Delta n^{(\mathrm{total})}$	Total refractive index change

1. INTRODUCTION

Recent developments in modern technology have given an opportunity to confine the electrons in semiconductor nanostructures [1-20]. If a thin layer of a narrower-band gap material is sandwiched between two layers of a wider-band gap material, a double heterojunction is formed. If narrower-band gap layer is sufficiently thin for *quantum properties* to be observed, then such a band alignment is called a *single quantum well.* The nanostructures with three-dimensional confinement of electrons and holes are called Quantum Dots (QDs).

When a thin layer of a semiconductor is grown on top of a substrate, which has a quite different lattice constant, the thin layer orders, or *self-assembles* into QDs. As a result, the energy levels are quantized and for that reason they are often referred as artificial atoms. The localized states are both for conduction- and valence-band carriers, and discrete interband transition energies appear between these so-called shells [21]. The description of the interaction with the light field is different for QDs than that of the atomic systems with single-electron excitations. [22-28]

QD is a region of space (1–100 nm at low temperatures) in a crystalline semiconductor matrix, with sizes comparable to the exciton Bohr radius a. QDs in AlGaAs based material have been obtained with radii typically in the range of 50 nm or larger. For such sizes the spacing between energy levels can be larger than the thermal energy. When kBT is smaller than the electron–hole binding energy due to Coulomb attraction, electrons and holes bind to form excitons, which can decay, generating light with spectra. In this limit, the electron-hole Coulomb interaction may be neglected and the calculation simplifies [25-27]. On the other hand, this interaction becomes important in the weak confinement limit. The importance of the interplay between the confinement and the Coulomb interaction is usually underlined in the literature.

Modern crystal growth techniques make it possible to grow layers of semiconductor material which are narrow enough to confine the electron motion in one dimension. In such

quantum-well structures, the electron wave functions are quantized like the standing waves of a particle in a square well potential.

These low-dimensional systems can be growth as quantum wells, quantum wires, and quantum dots which are effectively two, one and zero dimensional. In a quantum dot, the electron is confined in all three-dimensions, thus reducing the degrees of freedom to zero [13], [18-19].

The growth of semiconductor quantum dots was started by melting a certain amount of semiconductor material, such as ZnS or ZnSe together with the glass material and it is still one of the most used techniques. The synthesis of semiconductor crystallites in liquid solvents is one of the currently used techniques. These dots have been grown in a crystal matrix, inside ionic materials, in polymer films, etc., by different manufacturing processes; by melting and annealing processes, by sol-gel techniques. The epitaxially grown self-assembled QDs has been presently performed on a wide variety of semiconductor alloys such as Ge/Si, InAs/GaAs, (In,Ga)As/GaAs, (Ga,In)P/InP, CdSe/Zn(S,Se), and (In,Ga)N/GaN. The spectral region reaches from the near infrared ($\sim$ 1.5 μm) to the blue-green region ($\sim$ 430–500 nm). For self-assembled QDs one usually finds a strong confinement in growth direction [14], [17], [29].

Semiconductor QDs have very rich physics and their high potential for applications in photonics and quantum information technology has being attractive for the researchers. The QD is a model system in which we can study subjects from many different fields and these artificially made structures show interesting properties which are completely different from solid-state bulk materials. QDs have found various application areas especially microelectronic and optoelectronic devices [57]. The electronic structures, energy states, optical and other physical properties of QDs with one- and two-electrons have been commonly studied by using various calculation methods [9-11], [29-31].

The nonlinear optical properties of QD have the potential for device application such as infrared photo detectors, quantum dot lasers, high-speed electro-optical modulators, light emitting diodes, far-infrared laser amplifiers, one electron transistors, optical memory technology and other extensive applications in optics communication.

The communication technology also supports these studies for the need for faster optical switches and communication lines.

QDs can be used as triggered sources of single photons, where a classical pulse of light or of electric current is deterministically converted into a light quantum. This can be used in secure data transmission based on quantum cryptography [32-36], [37]. Excitons in QDs are used as two-level systems, i.e., quantum bits. Weak and strong-coupling of excitons and optical modes in these semiconductor micro-cavities allow solid-state-based quantum electrodynamics (QED) experiments [38].

The nonlinearity of the polarization of the medium is the main interest of scientific researches. Due to the existence of a quantum confinement effect, the nonlinear effects can be enhanced more strongly in these low-dimensional quantum systems than in bulk materials.

The nonlinear optical properties, including the optical absorption, linear and nonlinear changes in the refractive index and the third harmonic generation under an electric field have been studied in many works [39-41]. To investigate the optical properties of QDs, the system may be off-resonantly excited by an optical pulse. The nonlinear optical response depends strongly on the shape of the confining potential experienced by the charge carriers in the medium. Studies on different confining potentials are based on the better control of the atomic layers of the constituents which makes it possible to design QW and QDs with variable shapes [42-44]. Confinement can be controlled through the size and shape of the QDs. The effect of different confining potentials should also be studied from the perspective of optimizing nonlinear optical properties of these low dimensional systems. The other possible factors that may be included are the presence of impurties, strain, temperature etc..

A very large dipole strength and a narrow bandwith have been observed in the experiments for GaAs QDs which suggest that the intersubband optical transitions in QDs may have huge nonlinearities [51].

The nonlinear optical response increases strongly with the asymmetry in confinement profile and this asymmetry may be obtained by the application of an external electric field.

In the present work, we consider the electron confined in GaAs QDs assumed to be disc like and spherical shapes, where the degrees of freedom in the electron motion is zero. Infinitely deep and parabolic confining potentials are studied, including the optical absorption, linear and nonlinear changes in the refractive index.

The linear (first-order) and nonlinear (third-order) absorption coefficients and refractive index changes are analytically studied. These properties are examined by varying several parameters; QD shape and size, confinement potential, optical intensity, external electric field.

The nonlinear optical coefficients are calculated within the density matrix formalism. The electronic structure of the QDs is calculated using the effective mass approximation. Confinement is assumed to be strong and therefore the excitonic effects are neglected.

The calculated wavefunctions, energy eigenvalues, matrix elements, refractive index and the absorption coefficients all change appreciably with changing confinement, and the incident photon energies. Our results show that the changes in the refractive index and the optical absorption coefficient depend sensitively on the shape and size of the QDs and on the confinement potential. Maximum change in linear and nonlinear refractive index and maximum absorption coefficient are obtained in the spherical QD case than those obtained for the disc-like QD.

The results are in qualitative agreement with those in the literature. They present the possibility of the optimization of the absorption coefficient and refractive index using several relevant parameters. This conclusion may lead to improvement for industrial applications.

We also consider the effect of the applied electric field on the linear and nonlinear changes in the refractive index of the medium, for the infinitely deep confining potential case in disc-like and spherical QDs. The nonlinear optical properties increase as the strength of the

applied electric field and the optical intensity increase. One can engineer the structure of materials by means of external electric field and confinement strengths and tailors the energy spectrum to produce desirable nonlinear optical effects.

We present the theoretical framework in Section 2 with analytic expressions for the calculated quantities. The calculations are shown detaily in Section 3. The results are analyzed in Section 4. Finally, the Section 5 includes a brief summary of the findings.

2. THEORETICAL FRAMEWORK

Optical properties of materials may be modified using light photons, a laser light is sufficiently intense to modify. Nonlinear phenomena, such as second-harmonic, third-harmonic generations, occur when the response of a material to an applied field depends on the strength of the field nonlinearly [45].

The electric dipole approximation is used [46]. Using the fact that the wavelength of the incident radiation field is far longer than the QD dimensions, the incident electromagnetic field can be written as

$$E(t) = \sum_j E(\omega_j) e^{-i\omega_j t}, \tag{2.1}$$

where the summation goes over all frequencies of the optical radiation applied to the system.

Polarization $P(t)$ of a material, dipole moment per unit volume, depends on the strength of the applied field $E(t)$. In linear case, the polarization and the strength are linearly proportional but the nonlinear optical response of a material can be described more generally as;

$$P(t) = \chi^{(1)}E(t) + \chi^{(2)}E^2(t) + \chi^{(3)}E^3(t) + \cdots = \sum_j P(\omega_j) e^{-i\omega_j t}, \tag{2.2}$$

where $\chi^{(1)}$, $\chi^{(2)}$, and $\chi^{(3)}$ are the linear, second-order and third-order nonlinear optical susceptibilities, respectively.

Third-order nonlinear polarization is $P^{(3)}(t) = \chi^{(3)}E^3(t)$ and if Equation (2.1) is substituted, the expression for $\chi^{(3)}(\omega_r + \omega_q + \omega_p; \omega_r, \omega_q, \omega_p)$ contains 44 different terms provided that all the frequencies are distinct [45]. In this thesis, $\chi^{(3)}(\omega)$ which can be achieved by the permutations of the frequency set $(\omega, \omega, -\omega)$ is considered.

$\chi^{(3)}(\omega;\omega,-\omega,\omega)$ and $\chi^{(3)}(\omega;\omega,\omega,-\omega)$ are dominant at one-photon resonance and give significant contribution to the nonlinear refractive index and absorption coefficient [45], [47].

In this thesis, the linear and third-order nonlinear optical susceptibilities are mainly considered, since the linear, nonlinear refractive index and optical absorption coefficient are based on them. While the real part of optical susceptibility is related to the changes in refractive index, the imaginary part describes the absorption of radiation.

The frequency dependent refractive index is given by

$$n(\omega) = \mathrm{Re}[\sqrt{\epsilon + 4\pi\chi(\omega)}], \tag{2.3}$$

Then the change in the refractive index due to the incident field is written as

$$\Delta n(\omega) = \mathrm{Re}[\sqrt{2\pi\chi(\omega)/n_r}], \tag{2.4}$$

where ϵ is the static dielectric constant of the QD material and n_r is the refractive index. The change in the linear and the third-order nonlinear refractive index (RI) due to the incident field are given by [32-35, 48],

$$\Delta n^{(1)}(\omega) = \frac{1}{2\pi\varepsilon_o n_r} Re\left[\chi^{(1)}(\omega)\right], \tag{2.5}$$

$$\Delta n^{(3)}(\omega, I) = -\frac{1}{2\pi\varepsilon_o n_r} Re\left[\chi^{(3)}(\omega)\right], \tag{2.6}$$

and the change in the total RI is

$$\Delta n(\omega, I) = \Delta n^{(1)}(\omega) + \Delta n^{(3)}(\omega, I). \tag{2.7}$$

where $\varepsilon_o$is the permittivity of free space.

The total optical absorption coefficient is given by ,

$$\alpha(\omega, I) = \alpha^{(1)}(\omega) + \alpha^{(3)}(\omega, I), \tag{2.8}$$

where the linear absorption coefficient is

$$\alpha^{(1)}(\omega) = \frac{\omega}{n_r}\sqrt{\epsilon} Im\left[\chi^{(1)}(\omega)\right], \tag{2.9}$$

and the third-order nonlinear absorption coefficient

$$\alpha^{(3)}(\omega, I) = -\frac{\omega}{n_r}\sqrt{\epsilon} Im\left[\chi^{(3)}(\omega)\right]. \tag{2.10}$$

2.1. DENSITY MATRIX FORMALISM

Nonlinear optical susceptibility can be calculated using the density matrix formulation of quantum mechanics. It becomes particularly large when one of the frequencies of the incident field (or sum or differences) becomes equal to a transition frequency of the system, resonance response.

Density matrix formulation allows us to describe these near resonant situations, relaxation processes, thus it can tell us how accurately we need to set the incident field frequency to that of the system resonance and how strongly the system response at the resonance. This formalism provides more generally valid results [45, 48].

One can describe the physical properties of the atomic system at quantum state s in terms of the wavefunction $\psi_s(\vec{r}, t)$ which satisfies the time-dependent Schrödinger equation with the Hamiltonian H

$$H = H_o + V(t). \tag{2.11}$$

H_o is the Hamiltonian for free atom and $V(t)$ is the energy of interaction of the atom with external electromagnetic field (weak interaction).

$\psi_s(\vec{r},t)$ can be written as

$$\Psi_s(\vec{r},t) = \sum_n C_n^s(t)\Psi_n(\vec{r}), \tag{2.12}$$

where $\vec{r}$ is the position vector, $C_n^s(t)$ is the probability amplitude that the atom at state s is in energy eigenstate n at time t and $\Psi_n(\vec{r})$ is the eigensolution to the time independent Schrödinger equation

$$H_o\Psi_n(\vec{r}) = E_n\Psi_n(\vec{r}). \tag{2.13}$$

where

$$\int \Psi_m^*(\vec{r})\Psi_n(\vec{r})d^3r = \delta_{mn}. \tag{2.14}$$

The interaction Hamiltonian $V(t)$ has a general form

$$V(t) = -\vec{\mu}\cdot\vec{E}(t) \tag{2.15}$$

where $\vec{\mu} = -e\vec{r}$ is the electric dipole moment operator and $-e$ is the charge of the electron.

The polarization can also be written in terms of the expectation value of electric dipole moment $\mu(t)$, which can be calculated using the density matrix $\hat{\rho}$;

$$P(t) = N\langle\mu(t)\rangle = N\mathrm{tr}(\hat{\rho}\hat{\mu}) = N\sum_{nm}\rho_{nm}\mu_{mn}, \tag{2.16}$$

where N is the free electron density and $\langle\mu(t)\rangle = \sum_j\langle\mu(\omega_j)\rangle e^{-i\omega_j t}$. Indices n and m run over all of the energy eigenstates of the system.

The elements of the density matrix of a system is defined by

$$\rho_{nm} = \sum_s p(s)C_m^{s\,*}C_n^s, \tag{2.17}$$

with the probability $p(s)$ of a system being in the state s.

By direct time differentiation of Equation (2.17) and using Schrödinger's equation for the time evolution of the probability amplitudes [45], the density matrix equation of motion is obtained including damping terms (nonvanishing value of $dp(s)/dt$),

$$\frac{d\rho_{nm}}{dt} = \frac{1}{i\hbar}[H, \hat{\rho}]_{nm} - \Gamma_o\left(\rho_{nm} - \rho_{nm}^{(0)}\right), \tag{2.18}$$

assuming ρ_{nm} relaxes to its equilibrium value $\rho_{nm}^{(0)}$ at a single relaxation rate Γ_o only.

The iterative solution of Equation (2.18), [45], where $V(t)$ is replaced by $\lambda V(t)$ (with λ being perturbation strength between 0 and 1), gives the density matrix steady state solution $\rho_{nm}^{(0)}$ and the higher order corrections $\rho_{nm}^{(1)}$, $\rho_{nm}^{(2)}$ and so on.

Using

$$\langle\mu(t)\rangle = \sum_{nm} \rho_{nm}^{(1)} \mu_{mn}, \tag{2.19}$$

and

$$P^{(1)}(\omega_j) = N\langle\mu(\omega_j)\rangle = N\sum_{nm} \rho_{nm}\mu_{mn} = \chi^{(1)}(\omega_j)E(\omega_j) \tag{2.20}$$

the linear susceptibility can be obtained.

The calculations in Equation (2.19) and (2.20) can be carried to higher orders. Using the third-order correction $\rho_{nm}^{(3)}$ to the density matrix, the expression for the third-order nonlinear susceptibility can be defined. But these expressions can be simplified using the two-level atom approximation.

2.2. TWO LEVEL ATOM APPROXIMATION

In this study, one-electron density matrix formalism is considered for a two-level approximation of the system of QDs, where the two energy states, 0 for the ground state and 1 for the first excited state. Only these two states interact appreciably with the incident optical field [27,45].

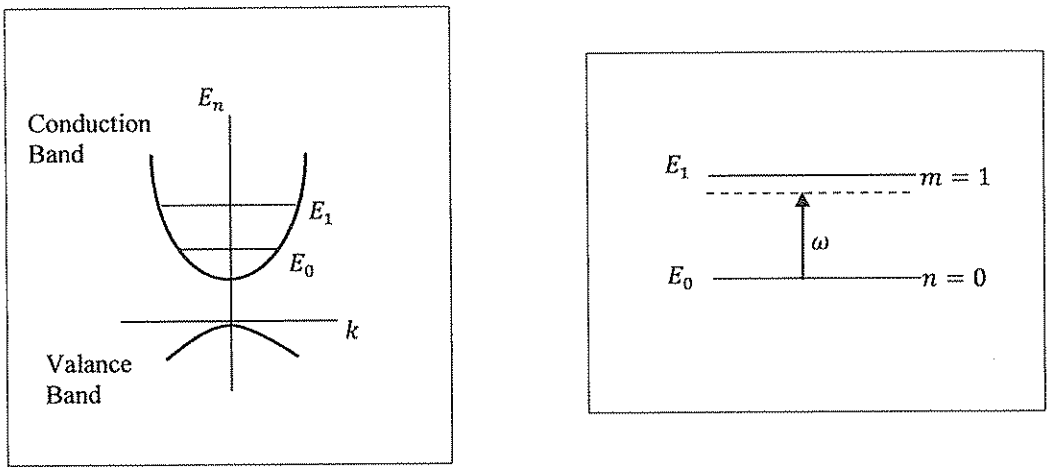

(a) (b)

Figure 2.1. (a) Schematic plot of the energies for electrons in QDs, (b) near-resonant excitation of the two level system.

When a transition of a material system is resonantly excited, it is usually adequate to deal only with the two atomic levels that are connected to the incident field and give resonance. When only two levels are included, the sums over all atomic states that appear in the density matrix formalism simplifies, $n = 0$ and $m = 1$. The density matrix is given by

$$\hat{\rho} = \begin{bmatrix} \rho_{00} & \rho_{01} \\ \rho_{10} & \rho_{11} \end{bmatrix}. \tag{2.21}$$

Dipole moment operator $\hat{\mu}$ is

$$\hat{\mu} = \begin{bmatrix} \mu_{00} & \mu_{01} \\ \mu_{10} & \mu_{11} \end{bmatrix}. \tag{2.22}$$

The diagonal elements of the dipole matrix is zero in symmetry cases, but they are non-zero if the symmetry is disturbed, e.g. applied external electric field.

Using the density matrix formalism and the two level approximation, the linear susceptibility is written as

$$\chi^{(1)}(\omega) = \frac{N|\mu_{10}|^2}{E_{10} - \hbar\omega - i\hbar\Gamma_o}, \tag{2.23}$$

where $E_{10} = E_1 - E_0$ is the energy difference between the two levels.

Third-order nonlinear susceptibility is

$$\chi^{(3)}(\omega, I) = \frac{2\pi I N|\mu_{10}|^4}{n_r c(E_{10} - \hbar\omega - i\hbar\Gamma_o)} \left[\frac{4}{(E_{10} - \hbar\omega)^2 + (\hbar\Gamma_o)^2} - \frac{|\mu_{11} - \mu_{00}|^2}{|\mu_{10}|^2} \frac{1}{(E_{10} - \hbar\omega - i\hbar\Gamma_o)(E_{10} - i\hbar\Gamma_o)} \right]. \tag{2.24}$$

The intensity I of the incident field is $I = \frac{1}{2}\varepsilon_o c E^2$, where c is the speed of light in vacuum.

2.3. EFFECTIVE MASS APPROXIMATION

The electronic structure of the QDs is calculated using the effective mass approximation. Electrons (or holes), that are free to move around the lattice of a semiconductor, experience the periodic variation of the Coulomb potential of the atoms. Bloch's theorem [27] offers the "effective mass" concept for the electron and thus the whole periodic crystal potential is lumped into this concept. The problem is then reduced to that of an electron in free space but the electron mass is taken to be the electron effective mass m^*.

The electron effective mass depends on the wavevector $\vec{k}$ and envelope wave function ψ_n of the electron is determined by solving the time independent Schrödinger equation

$$H\psi_n(\vec{r}) = E_n\psi_n(\vec{r}), \tag{2.25}$$

where E_n is the energy of the nth state. The eigenfunctions in Equation (2.13) is written as $\Psi_n(\vec{r}) = \psi_n(\vec{r})\exp(i\vec{k}\cdot\vec{r})$, Figure 2.2.

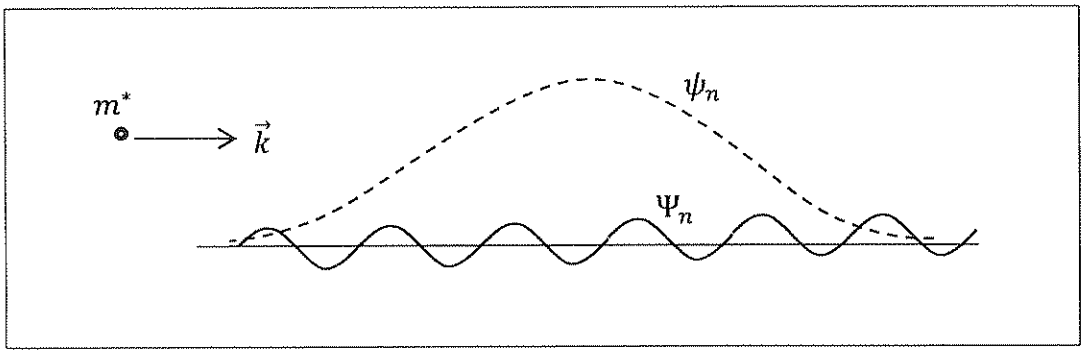

Figure 2.2. Effective Mass Approximation and envelope wavefunction

2.4. STARK EFFECT

If a one-electron atom is subjected to a uniform electric field $\vec{F}$ in a direction x, the Hamiltonian H splits into two parts as:

$$H = H_o + e|\vec{F}|x \tag{2.26}$$

where H_o is the unperturbed part of the total Hamiltonian, e is the absolute value of the electron charge and $\vec{F}$ is the external electric field. The second term in Equation (2.26) describes the interaction of an electromagnetic wave with the two-level electron system in the dipole approximation.

If the inequality

$$e\left|\vec{F}\right|x \ll \left|E_0^{(0)} - E_1^{(0)}\right| \tag{2.27}$$

is satisfied ($E_0^{(0)}$ and $E_1^{(0)}$ are unperturbed ground and first-excited state energies), we determine the new wavefunctions and the corresponding energy levels using the time-independent, non-degenerate perturbation theory [32-35, 46], such that;

$$E_n' = E_n^{(0)} + \Delta_n = E_n^{(0)} + e\left|\vec{F}\right|x_{nn} + + \left|\vec{F}\right|^2 \sum_{j\neq n} \frac{\left|\mu_{nj}\right|^2}{E_n^{(0)} - E_j^{(0)}} + \cdots \tag{2.28}$$

and

$$\psi_n' = \psi_n^{(0)} + \left|\vec{F}\right| \sum_{j\neq n} \psi_j^{(0)} \frac{\left|\mu_{nj}\right|}{E_n^{(0)} - E_j^{(0)}} + \cdots \tag{2.29}$$

where $\mu_{n,j} = \left\langle \psi_n^{(0)} \middle| -ex \middle| \psi_j^{(0)} \right\rangle$ and $\psi_0^{(0)}$is expected to be a parity eigenstate; hence, $x_{nn} = 0$. The matrix elements, μ_{nj}, are evaluated using the unperturbed wave functions.

3. CALCULATIONS

In this thesis, two different shapes of QDs are analysed, disc-like and spherical. And two types of confining potentials, infinitely deep and parabolic, are studied. Also the effect of external static field is considered. In each case, the linear and nonlinear susceptibilities, Equation (2.23) and Equation (2.24), are calculated. The electron-hole Coulomb interaction is neglected.

The numerical values in the present work are calculated for $GaAs/Al_xGa_{1-x}As$ QD with $x = 0.3$. The input parameters are taken as, the electron density $N = 5.0 \times 10^{22} m^{-3}$, effective mass of the electron $m^* = 0.067 m_e$, where m_e is the free electron mass and $\hbar = h/2\pi$.. The relaxation rate is taken as $\Gamma_0 = \frac{1}{0,14} ps$ and the dielectric constant is $\epsilon = 12.4$.

The optical radiation of various frequencies is considered, with polarization along the x-axis of the QDs. The matrix elements of the dipole operator, μ_{10}, μ_{00} and μ_{11}, are calculated using the related wave functions of the electron, $\mu_{i,j} = \langle \psi_i | -ex | \psi_j \rangle$ with $(i, j = 0,1)$, where x indicates the direction of polarization of the incident wave.

The necessary wave functions ψ, and energies E_1 and E_0 for the two states of the electron in QD are determined as follows (the integral calculations are carried via "*Wolfram Mathematica 7.0*"):

3.1. DISC-LIKE QD WITH INFINITELY DEEP CONFINING POTENTIAL

It is assumed that the electron is confined in a disc-like QD. We approximate the difference of the band gaps of the semiconductor dot and of the surronding material as an infinitely high potential barrier.

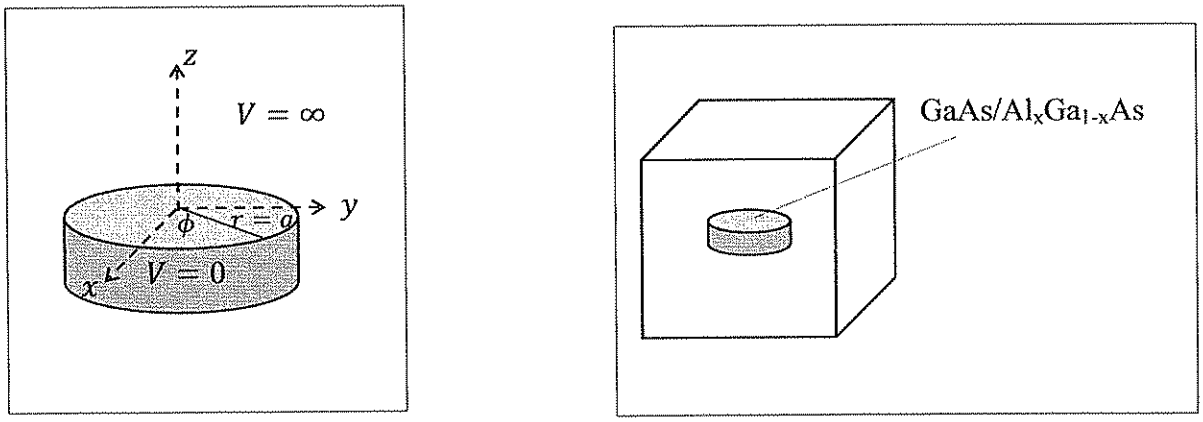

Figure 3.1. Diagram for the disc-like QD

The Hamiltonian operator in this system within the effective mass approximation is given by

$$H = -\frac{\hbar^2}{2m^*}\vec{\nabla}^2 + V, \tag{3.1}$$

And the confining potential is infinitely deep potential,

$$\begin{aligned} V &= \infty \qquad r > a, \\ V &= 0 \qquad r \leq a. \end{aligned} \tag{3.2}$$

In cylindrical coordinates, the Hamiltonian is written as

$$H = -\frac{\hbar^2}{2m^*}\left[\frac{1}{r}\frac{\partial}{\partial r}\left(r\frac{\partial}{\partial r}\right) + \frac{1}{r^2}\frac{\partial^2}{\partial \phi^2}\right] \tag{3.3}$$

is invariant with respect to the rotations about the z-axis of the disc with radius $a \gg z$. The degrees of freedom is zero.

One-electron envelope wave function is calculated by the method of separation of variables, using:

$$\psi(r,\phi) = R(r)\Phi(\phi). \tag{3.4}$$

By substituting Equation(3.4) into time indepent Schrödinger Equation $H\psi(r,\phi) = E\psi(r,\phi)$, we get

$$\left(\Phi\frac{1}{r}\frac{\partial}{\partial r}\left(r\frac{\partial R}{\partial r}\right) + \frac{R}{r^2}\frac{\partial^2\Phi}{\partial\phi^2}\right) + \frac{2m^*}{\hbar^2}E = 0. \tag{3.5}$$

Then dividing the Equation(3.5) by $\psi(r,\phi)$:

$$\left(\frac{1}{R}\frac{1}{r}\frac{\partial}{\partial r}\left(r\frac{\partial R}{\partial r}\right) + \frac{1}{r^2}\frac{1}{\Phi}\frac{\partial^2\Phi}{\partial\phi^2}\right) + \frac{2m^*}{\hbar^2}E = 0. \tag{3.6}$$

Taking the ϕ dependent terms to the right side of Equation (3.6) and setting the new equality to an arbitrary constant m^2, two independent equations are obtained as follows:

$$\frac{1}{\Phi}\frac{d^2\Phi}{d\phi^2} = -m^2, \tag{3.7}$$

and

$$\frac{1}{R}\frac{1}{r}\frac{d}{dr}\left(r\frac{dR}{dr}\right) + \frac{2m^*}{\hbar^2}E = m^2\,. \tag{3.8}$$

The Equation (3.7) is the harmonic oscillator equation [54] and the general solution is

$$\Phi_m(\phi) = Ce^{im\phi} \tag{3.9}$$

where C is an arbitrary constant and $m = 0, \pm1, \pm2, \pm3, ...$

The azimuthal angle ϕ changes between 0 and $2\,\pi$. The wave function must have a single value at both $\phi = 0$ and $\phi = 2\,\pi$. If we apply this condition:

$$\Phi(\phi + 2\,\pi) = \Phi(\phi) \tag{3.10}$$

then

$$Ce^{im(\phi+2\,\pi)} = Ce^{im\phi} \tag{3.11}$$

which implies that

$$e^{im2\pi} = 1 \tag{3.12}$$

the quantum number m is either zero or an integer.

The constant C can be determined via the normalization $C^2 \int_0^{2\pi} \Phi^* \, \Phi \, d\phi = 1$ and calculated as $C = \sqrt{\frac{1}{2\pi}}$. Then the exact solution of Equation (3.7) is written as

$$\Phi_m(\phi) = \sqrt{\frac{1}{2\pi}}\, e^{im\phi} \qquad \text{where } m = 0, \pm 1, \pm 2, \pm 3, \ldots \tag{3.13}$$

Setting $\lambda = \sqrt{\frac{2m^*}{\hbar^2} E}$ in Equation (3.8), this r dependent portion of the seperated equation is rearranged as:

$$r^2 \frac{d^2R}{dr^2} + r\frac{dR}{dr} + (\lambda^2 r^2 - m^2)R = 0 \tag{3.14}$$

This is of the same form as "Bessel's differential equation" which is a second order differential equation. So, there must be linearly independent solutions given in general form [49], [50].

$$R_m(r) = A\,J_m(\lambda r) + B N_m(\lambda r) \tag{3.15}$$

where $J_m(\lambda r)$ is the Bessel function of the first kind " cylindrical harmonics" and $N_m(\lambda r)$ is the Neumann function, of order m.

Since, the solution must be finite at $\lambda r = 0$, but $N_m(0) \to \infty$, the coefficient B must be taken as zero. Then ;

$$R_m(r) = A\,J_m(\lambda r). \tag{3.16}$$

Using the boundary condition $\psi(r,\phi) = 0$ at $r = a$,

$$R_m(a) = A\,J_m(\lambda a) = 0, \tag{3.17}$$

the condition $J_m(\lambda a) = 0$ requires the argument of J_m to be a zero of the Bessel's function. The zeroes, or roots, are the values of $x = \lambda r$, where $J_m(x)$ goes to zero. Bessel function of the first kind has an infinite number of roots, Figure 3.2.

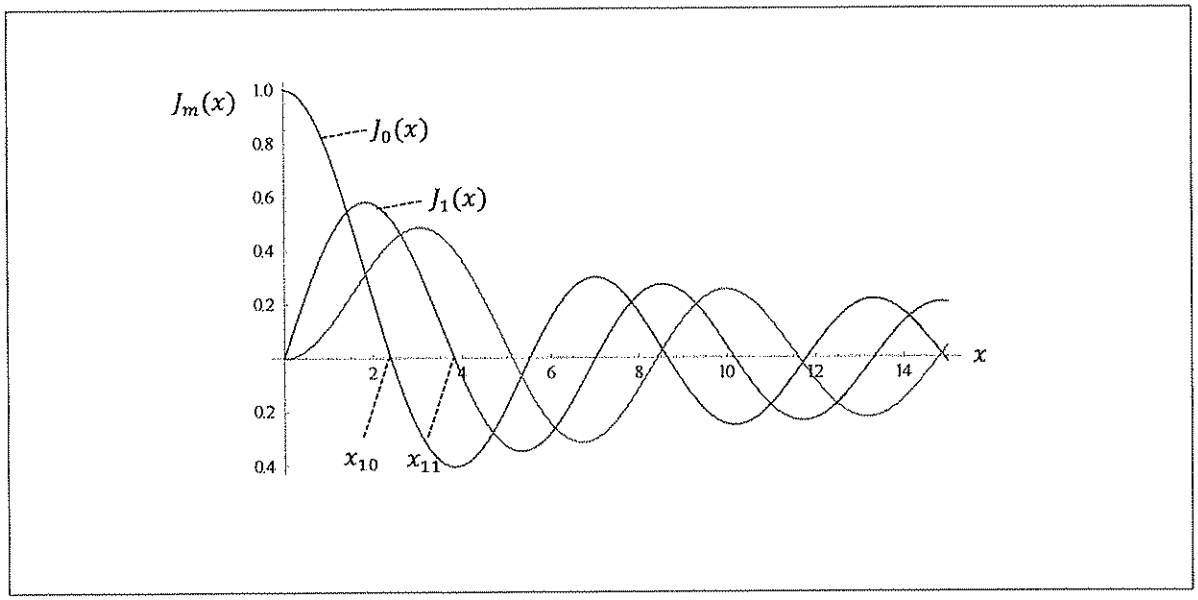

Figure 3.2. Bessel's function of the first kind.

With $x_{n,m}$ being the nth zero of the mth order Bessel's function, Equation (3.17) gives

$$\lambda = x_{n,m}/a \tag{3.18}$$

The wave function $R\ (r)$ is rewritten as

$$R_m\ (r)\ = A_m\, J_m\left(\frac{x_{n,m}}{a}r\right) \tag{3.19}$$

For the disc-like QD system, the two-level approximation is used, $m = 0$ represents the ground state of the system and $m = 1$ is the first excited state.

The normalization integral $A_m^2 \int_0^{2\pi} J_m\left(\frac{x_{n,m}}{a}r\right) J_m\left(\frac{x_{n,m}}{a}r\right) = 1$ gives the constants A_0 and A_1 for $m = 0$ and $m = 1$:

For m = 1(excited state)	***For m = 0 (ground state)***
$\psi_1(r,\phi) = R_1(r)\ \Phi_1(\phi)$ $\Phi_1\ (\phi) = \sqrt{\frac{1}{2\pi}}\, e^{i\phi}$	$\psi_0(r,\phi) = R_0(r)\ \Phi_0(\phi)$ $\Phi_0\ (\phi) = \sqrt{\frac{1}{2\pi}}$
$R_1(r) = A_1\, J_1\left(\frac{x_{1,1}}{a}r\right)$ $x_{1,1} = 3.83171$ $\int_0^a A_1{}^2\, J_1\left(\frac{3.83171}{a}r\right) J_1\left(\frac{3.83171}{a}r\right) \mathrm{d}r = 1$ $A_1{}^2(0.0811074a) = 1$ $A_1 = \frac{3.51131}{a}$	$R_0(r) = A_0\, J_0\left(\frac{x_{1,0}}{a}r\right)$ $x_{1,0} = 2.40483$ $\int_0^a A_0{}^2\, J_0\left(\frac{2.40483}{a}r\right) J_0\left(\frac{2.40483}{a}r\right) \mathrm{d}r = 1$ $A_0{}^2(0.13475a) = 1$ $A_0 = \frac{2.72411}{a}$

Using Equation (3.13) and Equation (3.19), the complete wavefunctions, Equation (3.4), are calculated as:

$$\psi_0(r,\phi) = \frac{2{,}72411}{\sqrt{2\pi\eta a_o^*}}\ J_0\left(\frac{2.40483}{\eta a_o^*}r\right), \tag{3.20}$$

and

(3.21)

where is the effective Bohr radius and is the Bohr radius.

In Figure (3.2), the squared wavefunctions, and are plotted for two different sizes of the disc-like QD, for and . The radius of the disc-like QD is controlled by the parameter where the radius . The smaller the value of , the smaller the disc-like QD, then the wavefunction has an increased peak and sharpens as in Figure (3.3).

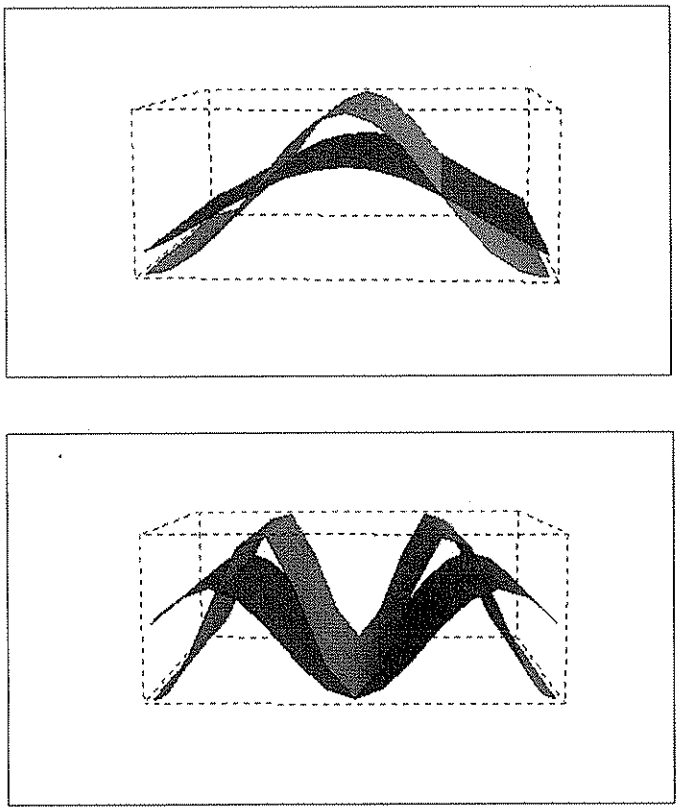

Figure 3.3. Diagram for the probability densities and of the electron confined in disc-like QD, infinitely deep potential

The related energy states, for the ground state and for the first excited state, can be found using the definition together with Equation (3.18).

$$E_{n,m} = \frac{x_{n,m}^2 \hbar^2}{2m^*(\eta a_o^*)^2}. \tag{3.22}$$

The transition energy $E_{10} = E_{1,1} - E_{1,0} = E_1 - E_0$ for the disc-like QD with infinetely deep confining potential is then calculated as

$$E_{10} = \frac{1}{\eta^2}\frac{\hbar^2}{2m^*(a_o^*)^2}\left(x_{1,1}^2 - x_{1,0}^2\right) = \frac{1}{\eta^2}(8.11)eV = \frac{1}{\eta^2}(1.29 \times 10^{-18}J) \tag{3.23}$$

where $x_{1,1} = 3.83171$ and $x_{1,0} = 2.40483$ and $\frac{\hbar^2}{2m^*(a_o^*)^2} = 0.91\ eV$.

Energy E_{10} increases as the QD size decreases.

Taking $x = rcos\phi$ as the direction of polarization of the incident wave, the necessary dipole matrix elements are determined.

The diagonal elements of the dipole matrix are calculated as zero:

$$\mu_{00} = \langle\psi_0|-ercos\phi|\psi_0\rangle = 0, \tag{3.24}$$

$$\mu_{11} = \langle\psi_1|-ercos\phi|\psi_1\rangle = 0, \tag{3.25}$$

and

$$\mu_{10} = \langle\psi_1|-ex|\psi_0\rangle$$

$$= \langle\psi_1(r,\phi)|-ercos\phi|\psi_0(r,\phi)\rangle.$$

Then, the dipole matrix element μ_{10} is:

$$\mu_{10} = -e\iint_0^a \left[\frac{3.51131}{\sqrt{2\pi\eta a_o^*}}\ J_1\left(\frac{3.83171}{\eta a_o^*}r\right)e^{i\phi}\right]\left[\frac{2,72411}{\sqrt{2\pi\eta a_o^*}}\ J_0\left(\frac{2.40483}{\eta a_o^*}r\right)\right] rcos\phi rdrd\phi. \tag{3.26}$$

Using Equation (3.26), the element of the dipole matrix μ_{10} is calculated as

$$\mu_{10} = -\eta(\,2.49 \times 10^{-29}\mathrm{C.m.}), \tag{3.27}$$

for the disc-like QD with infinetely deep confining potential.

3.1.1. Stark Effect On The Disc-Like QD With Infinitely Deep Confining Potential

The uniform electric field $\vec{F}$ in $x = rcos\phi$ direction is studied and the field strengths chosen in this study satisfy the condition given in Equation (2.27).

The applied field values such as 5.0 kV/cm satisfies

$$e|\vec{F}|rcos\phi \ll \left|E_0^{(0)} - E_1^{(0)}\right| = \left|E_{10}^{(0)}\right|, \tag{3.28}$$

where $E_{10}^{(0)} = \frac{1}{\eta^2}(1.29 \times 10^{-18}J)$.

Using Equation (2.28) with Equations (3.22), (3.23) and (3.27), perturbed ground state energy E_0' is written as

$$E_0' = \frac{1}{\eta^2}\frac{\hbar^2}{2m^*(a_o^*)^2}x_{1,0}^2 + \left|\vec{F}\right|^2 \frac{|\mu_{10}|^2}{\frac{1}{\eta^2}\frac{\hbar^2}{2m^*(a_o^*)^2}(x_{1,0}^2 - x_{1,1}^2)}, \tag{3.29}$$

and perturbed first-excited state energy E_1' is

$$E_1' = \frac{1}{\eta^2}\frac{\hbar^2}{2m^*(a_o^*)^2}x_{1,1}^2 + \left|\vec{F}\right|^2 \frac{|\mu_{10}|^2}{\frac{1}{\eta^2}\frac{\hbar^2}{2m^*(a_o^*)^2}(x_{1,1}^2 - x_{1,0}^2)}. \tag{3.30}$$

The energy difference between the two states of the electron is now $E_{10}' = E_1' - E_0'$.

The perturbed energies are found to be very close to their unperturbed values, such as for $\eta = 10$ and $F = 10\ kV/cm$, perturbed ground state energy was found to be $E'_{10} = 0.08122\ eV$ where as the unperturbed ground state energy was $E_{10} = 0.08108\ eV$.

And using Equation (2.29) with Equations (3.20), (3.21) and (3.27), the perturbed wave functions are written as,

$$\psi'_0 = \frac{2{,}72411}{\sqrt{2\pi\eta a_o^*}}\ J_0\left(\frac{2.40483}{\eta a_o^*}r\right) + |\vec{F}|\frac{|\mu_{10}|}{\frac{1}{\eta^2}\frac{\hbar^2}{2m^*(a_o^*)^2}(x_{1,0}^2 - x_{1,1}^2)}\left(\frac{3.51131}{\sqrt{2\pi\eta a_o^*}}\ J_1\left(\frac{3.83171}{\eta a_o^*}r\right)e^{i\phi}\right) \quad (3.31)$$

$$\psi'_1 = \frac{3.51131}{\sqrt{2\pi\eta a_o^*}}\ J_1\left(\frac{3.83171}{\eta a_o^*}r\right)e^{i\phi} + |\vec{F}|\frac{|\mu_{10}|}{\frac{1}{\eta^2}\frac{\hbar^2}{2m^*(a_o^*)^2}(x_{1,0}^2 - x_{1,1}^2)}\left(\frac{2{,}72411}{\sqrt{2\pi\eta a_o^*}}\ J_0\left(\frac{2.40483}{\eta a_o^*}r\right)\right). \quad (3.32)$$

The perturbed dipole matrix elements are calculated using Equations (3.31) and (3.32);

$$\mu'_{00} = \langle\psi'_0|-er\cos\phi|\psi'_0\rangle, \quad (3.33)$$

$$\mu'_{11} = \langle\psi'_1|-er\cos\phi|\psi'_1\rangle, \quad (3.34)$$

$$\mu'_{10} = \langle\psi'_1|-er\cos\phi|\psi'_0\rangle. \quad (3.35)$$

In this case, μ'_{00} and μ'_{11} are non-zero, since the potential is no longer symmetrical. Then the second term in the third-order susceptibility, in Equation (2.24), is also non-zero, it gives a positive contribution to the refractive index change and the absorption coefficient as the strength of the field increases.

3.2 DISC-LIKE QD WITH PARABOLIC CONFINING POTENTIAL

An electron is considered in a disc-like QD (with radius $a = \eta a_o^*$) with a parabolic confining potential and without the external electric field.

The Hamiltonian operator in this system within the effective mass approximation is given by

$$H = -\frac{\hbar^2}{2m^*}\left[\frac{1}{r}\frac{\partial}{\partial r}\left(r\frac{\partial}{\partial r}\right) + \frac{1}{r^2}\frac{\partial^2}{\partial \phi^2}\right] + V(r), \tag{3.36}$$

where the parabolic potential V is

$$V(r) = \frac{1}{2}m^*\omega_0^2 r^2, \tag{3.37}$$

where $\vec{r}$ is the position vector of the electron and ω_0 is the frequency of the parabolic confining potential.

Time-independent Schrödinger Equation is written as,

$$\left(\frac{1}{r}\frac{\partial}{\partial r}\left(r\frac{\partial \psi}{\partial r}\right) + \frac{1}{r^2}\frac{\partial^2 \psi}{\partial \phi^2}\right) - \frac{2m^*}{\hbar^2}(V - E)\psi = 0. \tag{3.38}$$

The method of separation of variables is applied and setting

$$\psi(r, \phi) = R(r)\Phi(\phi). \tag{3.39}$$

into Equation (3.38), the ϕ dependent normalized wave function is found as $\Phi_m(\phi) = \frac{1}{\sqrt{2\pi}}e^{im\phi}$, $m = 0, \pm 1, \pm 2, \pm 3, \ldots$.

Setting $\lambda = \sqrt{\frac{2m^*}{\hbar^2}E}$ and $k = \sqrt{\frac{m^{*2}\omega_0^2}{\hbar^2}}$ in the r dependent portion of the seperated equation:

$$r^2\frac{d^2R}{dr^2} + r\frac{dR}{dr} + (\lambda^2 r^2 - k^2 r^4 - m^2)R = 0. \tag{3.40}$$

Taking $\xi = \sqrt{k}r$ and making

$$R(\xi) = e^{-\xi^2/2}\gamma(\xi), \tag{3.41}$$

transformation, Equation (3.40) takes the form:

$$\frac{d^2\gamma}{d\xi^2} + \left(\frac{1}{\xi} - 2\xi\right)\frac{d\gamma}{d\xi} + \left(\frac{\lambda^2}{k} - 2 - \frac{m^2}{\xi^2}\right) = 0. \tag{3.42}$$

If $\gamma(\xi) = \xi^m v(\xi)$ and $b = \xi^2$, then Equation (3.42) can be written as

$$b\frac{d^2v}{db} + (m + 1 - b)\frac{dv}{db} + nv = 0. \tag{3.43}$$

where $n = \left(\frac{\lambda^2}{2k} - 1 - m\right)/2$.

This is associated "Laguerre differential equation" [49], and the solution is

$$L_n^m(\xi^2) = L_n^m\left(\frac{m^*\omega_0}{\hbar}r^2\right). \tag{3.44}$$

The normalized wave functions can be written as,

$$\psi_{s,m}(r,\phi) = \frac{1}{\sqrt{\pi}}\sqrt{\frac{n!}{(n+m)!}}\, e^{-\frac{m^*\omega_0}{2\hbar}r^2}\left(\sqrt{\frac{m^*\omega_0}{\hbar}}r\right)^m L_n^m\left(\frac{m^*\omega_0}{\hbar}r^2\right)e^{im\phi}, \tag{3.45}$$

with $s = 0,1$, $m = 0,1$ and $n = 0,1/2$ for the two-level system of disc-like QD.

Energies of the ground state and the first excited states [40] are found using

$$E_s = (s + 1)\hbar\omega_0. \tag{3.46}$$

Effective "dot size" is characterized by the frequency of oscillating electron in the QD, and it is defined as $L = a = \eta a_o^* = \sqrt{\hbar/m^*\omega_o}$

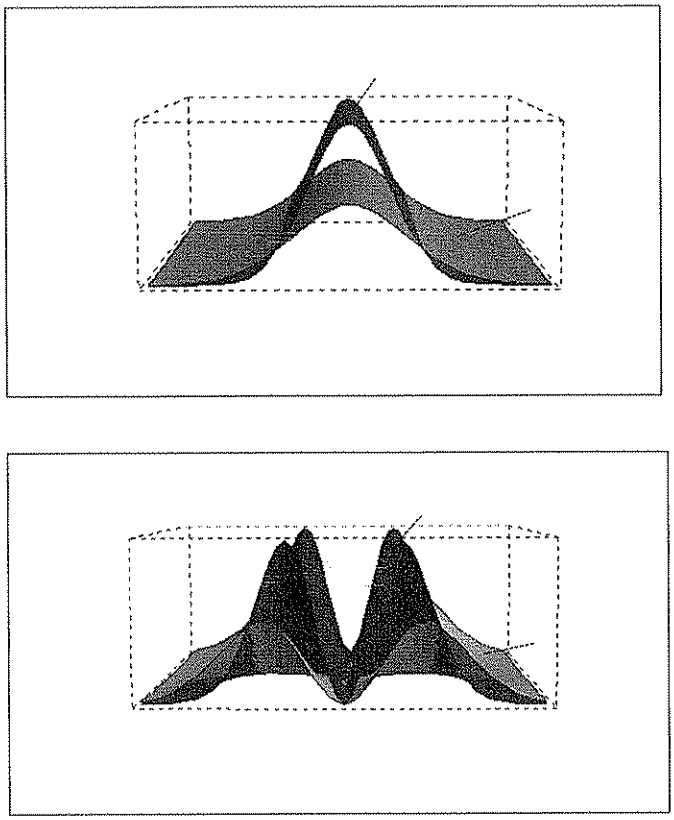

Figure 3.4. Diagram for the probability densities and of the electron confined in disc-like QD, parabolic potential.

The stronger the oscillation of the electron (large), the smaller the value of , thus the smaller the disc-like QD, then the wavefunction has an increased peak and sharpens as in Figure (3.4).

3.3 SPHERICAL QD WITH INFINITELY DEEP CONFINING POTENTIAL

The electron is confined in a QD assumed spherical in shape with radius . We approximate the difference of the band gaps of the semiconductor dot and of the surronding material as an infinitely high potential barrier.

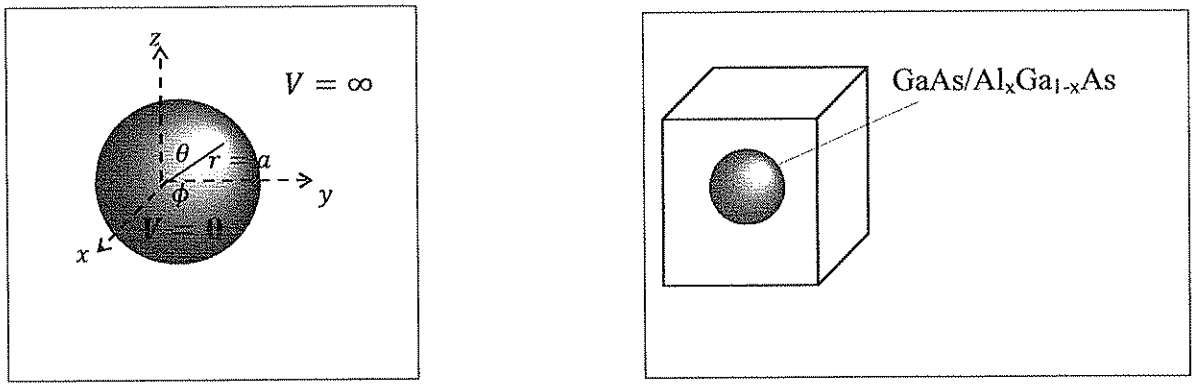

Figure 3.5. Diagram for the spherical QD.

and the confining potential is infinitely deep potential,

$$V = 0 \qquad r \leq a,$$
$$V = \infty \qquad r > a. \tag{3.47}$$

In spherical coordinates, the Hamiltonian is written as

$$H = -\frac{\hbar^2}{2m^*}\left[\frac{1}{r^2}\frac{\partial}{\partial r}\left(r^2\frac{\partial}{\partial r}\right) + \frac{1}{r^2 sin\theta}\frac{\partial}{\partial\theta}\left(sin\theta\frac{\partial}{\partial\theta}\right) + \frac{1}{r^2 sin^2\theta}\frac{\partial^2}{\partial\phi^2}\right., \tag{3.48}$$

One-electron envelope wave function is calculated by the method of separation of variables, using:

$$\psi(r,\theta,\phi) = R(r)Y(\theta,\phi). \tag{3.49}$$

By substituting Equation(3.49) into time indepent Schrödinger Equation $H\psi(r,\theta,\phi) = E\psi(r,\theta,\phi)$, we get

$$\frac{1}{R}\frac{d}{dr}\left(r^2\frac{dR}{dr}\right) + \frac{2m^*}{\hbar^2}r^2E = l(l+1), \tag{3.50}$$

$$sin\theta \frac{\partial}{\partial\theta}\left(sin\theta \frac{\partial Y}{\partial\theta}\right) + \frac{\partial^2 Y}{\partial\phi^2} = -l(l+1)Y sin^2\theta, \tag{3.51}$$

and setting

$$Y(\theta,\phi) = \Theta(\theta)\Phi(\phi), \tag{3.52}$$

θ and ϕ dependent terms can be seperated, here are the seperated equations,

$$\frac{1}{\Phi}\frac{d^2\Phi}{d\phi^2} = -m^2, \text{ and} \tag{3.53}$$

$$\frac{1}{\Theta} sin\theta \frac{d}{d\theta}\left(sin\theta \frac{d\Theta}{d\theta}\right) + l(l+1)sin^2\theta = m^2. \tag{3.54}$$

The solution of Equation (3.53) was given in Equation (3.9). And the condition given in Equation (3.10) requires that m is zero or an integer.

The solutions of Equation (3.51) and (3.54), [48-50], are:

$$R(r) = AJ_l(\lambda r), \tag{3.55}$$

and

$$\Theta(\theta) = BP_l^m(cos\theta). \tag{3.56}$$

where $J_l(\lambda r)$ is the "Spherical Bessel's Function" of order l and $\lambda = \sqrt{\frac{2m^*}{\hbar^2}E}$ and $P_l^m(cos\theta)$ is the associated Legendre Function.

With $x_{n,l}$ being the nth zero of the lth order spherical Bessel's function, $R_l(a) = A\,J_l(\lambda a) = 0$ gives

$$\lambda = x_{n,l}/a. \tag{3.57}$$

The wave function $R\ (r)$ is rewritten as

$$R_l\ (r)\ = A_l\, J_l\left(\frac{x_{n,l}}{a} r\right). \tag{3.58}$$

The constants A, B and C can be determined using normalization integrals and the resultant wave function of the electron is written as:

$$\psi_{n,l,m}(r,\theta,\phi) = \sqrt{\frac{2}{a^3}}(-1)^m \sqrt{\frac{(2l+1)!(l-|m|)!}{4\pi(l+|m|)!}}\, e^{im\phi} P_l^m(cos\theta)\, \frac{J_l(\lambda r)}{J_{l+1}(\lambda a)}, \tag{3.59}$$

where $n = 1,2 \ldots,\ l = 0,1,2 \ldots (n-1)$ and $m = -l, \ldots, 0, \ldots + l$.

For the ground state wavefunction of the electron confined in the spherical QD (infinitely deep potential), taking $n = 1,\ l = 0$ and $m = 0$ in Equation (3.59), the expression is written as

$$\psi_{1,0,0} = \frac{1}{\sqrt{2\pi\eta a_o^*}} \frac{sin\left(\frac{\pi}{\eta a_o^*} r\right)}{r}, \tag{3.60}$$

and taking $n = 1$, $l = 1$ and $m = 0$ in Equation (3.59), the first excited state wave function is determined as,

$$\psi_{1,1,0} = \sqrt{\frac{3\eta a_o^*}{\pi}}(0.227)\left[sin\left(\frac{4.49}{\eta a_o^*} r\right) - \left(\frac{4.49}{\eta a_o^*} r\right)\cos\left(\frac{4.49}{\eta a_o^*} r\right)\right]\frac{cos\theta}{r^2}, \tag{3.61}$$

where $\lambda a = 4.49$ is the first zero of the Spherical Bessel's function $J_1(\lambda r)$.

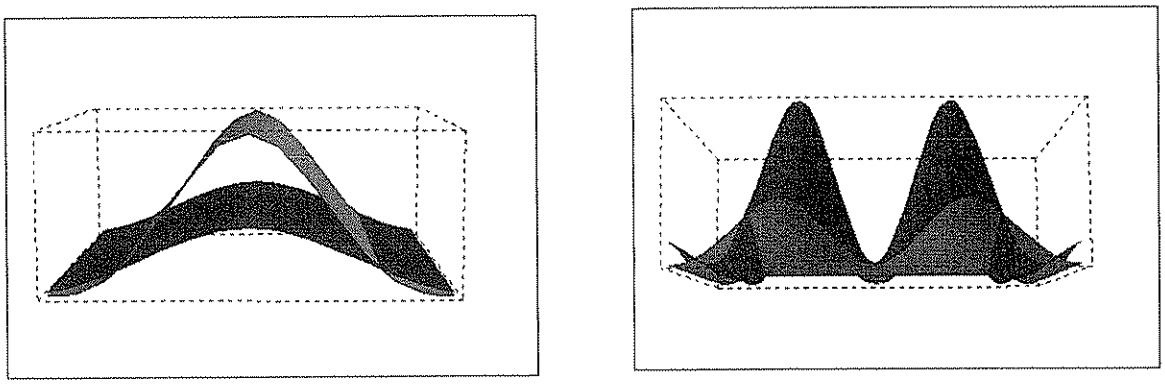

Figure 3.6. Diagram for the probability densities and of the electron confined in spherical QD, infinitely deep potential.

The related energy states, for the ground state and for the first excited state, can be found using the definition together with Equation (3.18).

(3.62)

The transition energy for the spherical QD with infinetely deep confining potential is then calculated as

(3.63)

This energy difference is higher than that calculated for the disc-like QD in Equation (3.23).

Taking as the direction of polarization of the incident wave, the elements of the dipole matrix are calculated as:

(3.64)

$$\mu_{11} = \langle \psi_{1,1,0} | -ercos\theta | \psi_{1,1,0} \rangle = 0, \tag{3.65}$$

and

$$\mu_{10} = \langle \psi_{1,1,0} | -ercos\theta | \psi_{1,0,0} \rangle. \tag{3.66}$$

Using Equation (3.66), the element of the dipole matrix μ_{10} is calculated as

$$\mu_{10} = -\eta\ (5.46 \times 10^{-29} \mathrm{C.m.}), \tag{3.67}$$

for the spherical QD with infinetely deep confining potential. The value of μ_{10} for the spherical QD is higher than that calculated for the disc-like QD in Equation (3.27).

3.3.1. Stark Effect On The Spherical QD With Infinitely Deep Confining Potential

The uniform electric field $\vec{F}$ in $z = rcos\theta$ is applied to the spherical QD, satisfying the condition given in Equation (3.27).

Using Equation (2.28) with Equations (3.62), (3.63) and (3.67), perturbed ground state energy E_0' is written as

$$E_0' = \frac{1}{\eta^2} \frac{\hbar^2}{2m^*(a_o^*)^2} x_{1,0}^2 + \left|\vec{F}\right|^2 \frac{|\mu_{10}|^2}{\frac{1}{\eta^2} \frac{\hbar^2}{2m^*(a_o^*)^2} (x_{1,0}^2 - x_{1,1}^2)}, \tag{3.68}$$

and perturbed first-excited state energy E_1' is

$$E_1' = \frac{1}{\eta^2} \frac{\hbar^2}{2m^*(a_o^*)^2} x_{1,1}^2 + \left|\vec{F}\right|^2 \frac{|\mu_{10}|^2}{\frac{1}{\eta^2} \frac{\hbar^2}{2m^*(a_o^*)^2} (x_{1,1}^2 - x_{1,0}^2)}. \tag{3.69}$$

where the first zeros of the spherical Bessel's functions J_0 and J_1 are $x_{1,0} = \pi$ and $x_{1,1} = 4.49$, respectively.

And using Equation (2.29) with Equations (3.62), (3.63) and (3.67), the perturbed wave functions are written as,

$$\psi'_{1,0,0} = \psi'_0 = \frac{1}{\sqrt{2\pi\eta a_o^*}} \frac{sin\left(\frac{\pi}{\eta a_o^*} r\right)}{r} +$$

$$|\vec{F}| \frac{|\mu_{10}|}{\frac{1}{\eta^2} \frac{\hbar^2}{2m^*(a_o^*)^2}(x_{1,0}^2 - x_{1,1}^2)} \left(\sqrt{\frac{3\eta a_o^*}{\pi}} (0.227) \left[sin\left(\frac{4.49}{\eta a_o^*} r\right) - \left(\frac{4.49}{\eta a_o^*} r\right) \cos\left(\frac{4.49}{\eta a_o^*} r\right) \right] \frac{cos\theta}{r^2} \right) \quad (3.70)$$

$$\psi'_{1,1,0} = \psi'_1 = \sqrt{\frac{3\eta a_o^*}{\pi}} (0.227) \left[sin\left(\frac{4.49}{\eta a_o^*} r\right) - \left(\frac{4.49}{\eta a_o^*} r\right) \cos\left(\frac{4.49}{\eta a_o^*} r\right) \right] \frac{cos\theta}{r^2} +$$

$$|\vec{F}| \frac{|\mu_{10}|}{\frac{1}{\eta^2} \frac{\hbar^2}{2m^*(a_o^*)^2}(x_{1,1}^2 - x_{1,0}^2)} \left(\frac{1}{\sqrt{2\pi\eta a_o^*}} \frac{sin\left(\frac{\pi}{\eta a_o^*} r\right)}{r} \right). \quad (3.71)$$

The perturbed dipole matrix elements are calculated using Equations (3.70) and (3.71);

$$\mu'_{00} = \langle \psi'_0 | -ercos\theta | \psi'_0 \rangle, \quad (3.72)$$

$$\mu'_{11} = \langle \psi'_1 | -ercos\theta | \psi'_1 \rangle, \quad (3.73)$$

$$\mu'_{10} = \langle \psi'_1 | -ercos\theta | \psi'_0 \rangle. \quad (3.74)$$

4. NUMERICAL RESULTS AND DISCUSSION

We present the numerical results for the parameters appropriate to a GaAs/$Al_xGa_{1-x}As$ QD with $x = 0.3$ [40] and take

$$N = 5.0\times10^{22}m^{-3}, \Gamma_0 = \frac{1}{0.14}ps^{-1}, n_r = 3.2, m^* = 0.067m_e,$$

where N is the three dimensional electron density, Γ_0 is the decay rate and m_e is the bare electron mass, the dielectric constant is taken as $\epsilon = 12.4$. The electron concentrations depend on the position of the Fermi level. The correct handling of this dependence on the external probes is properly done in earlier investigations [34,38,39].

The first and third-order susceptibility Equations (2.23) and (2.24), strongly depends on the energy difference E_{10} and the dipole matrix elements μ_{00}, μ_{11} and μ_{00}. They change with the shape and size of the QD, with the confining potential and also with the effect of external uniform electric field, hence the nonlinear optical response of these low dimensional systems depends strongly on these effects.

In Figure 4.1, the energies of the ground state E_0 and that of the first excited state E_1 are plotted as a function of the size of the disc-like and in Figure 4.2 for the spherical QD, with infinitely deep confining potential. The parameter η controls the size of QDs, as η increases so does the dot size. The energy values are higher in the spherical QD case, compared to those in the disc-like QD. The difference between the energies of these states E_{10} decreases with increasing QD size.

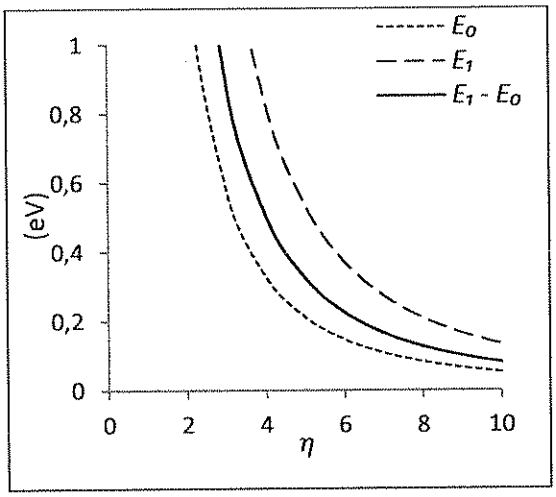

Figure 4.1. The energies of ground and excited states as a function of dot size parameter η for the disc-like, infinitely deep confining potential, no external field.

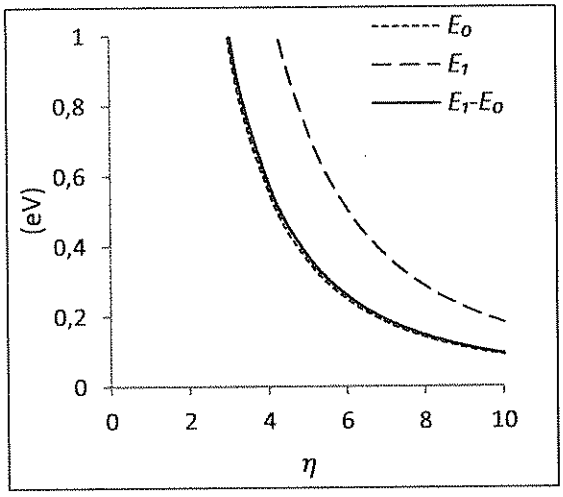

Figure 4.2. The energies of ground and excited states as a function of dot size parameter η for the spherical QD, infinitely deep confining potential, no external field.

The energy difference E_{10} is larger in the spherical QD than that in the disc-like case, as seen in Figure 4.3.

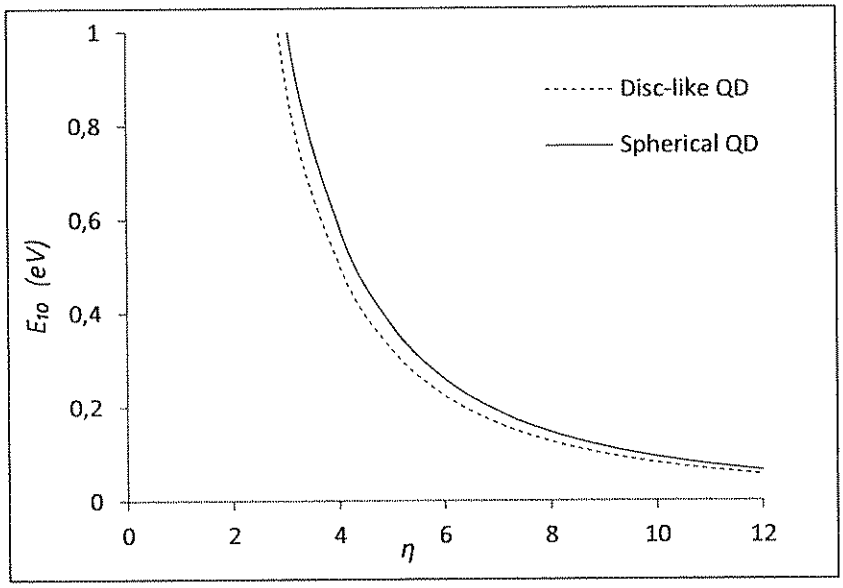

Figure 4.3. Effect of the QD shape on E_{10}, infinitely deep confining potential, no external field.

Figure 4.4 shows the energies E_0, E_1 and E_{10} as a function of η and of frequency ω_0, the parabolic confining potential in the disc-like QD. The dot size decreases with increasing frequency ω_0, with the equation $a = \eta a_o^* = \sqrt{\hbar/m^*\omega_o}$. As the oscillation of the confined electron increases with ω_0, the energy difference E_{10} also increases.

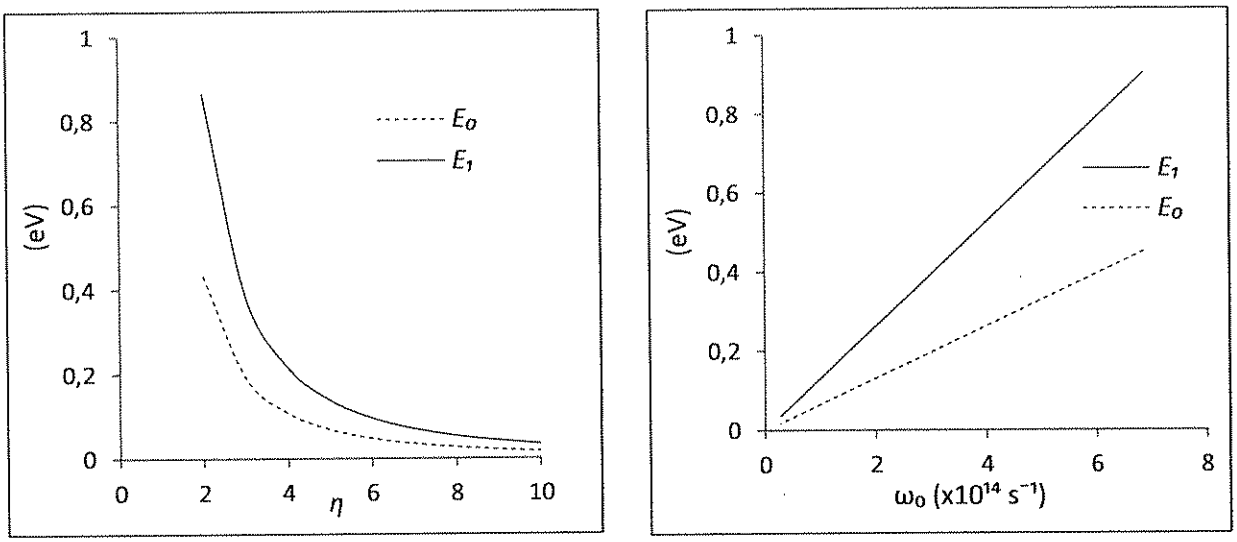

(a) (b)

Figure 4.4. E_0 and E_1 as a function of (a) η and (b) ω_0, disc-like QD, parabolic potential, no external field.

For the disc-like QD, the energy difference E_{10} is larger in the infinitely deep potential case than that obtained for the parabolic potential. The confinement potentials are effective on the value of E_{10}, this is clearly seen in Figure 4.5.

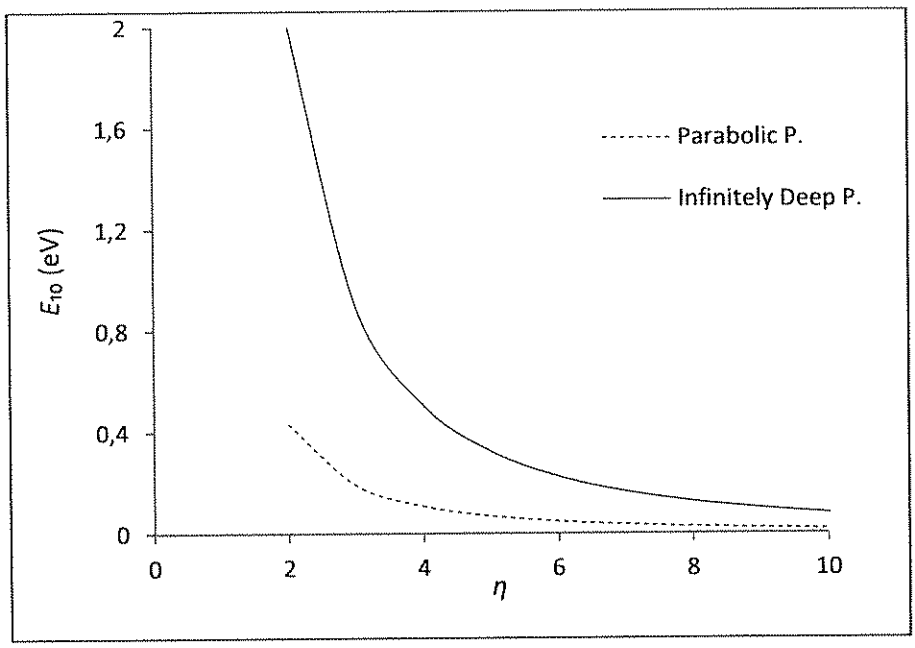

Figure 4.5. Effect of the confining potential on E_{10}, disc-like QD, no external field.

The difference between the unperturbed energy difference E_{10} and the perturbed one E'_{10}, calculated in the "Stark effect" cases, Section 3.1.1. and 3.3.1, could not be illustrated clearly on graphs but the values for different dot sizes and for different applied electric fields are listed in Table 4.1 and in Table 4.2, respectively. External field slightly increases the difference in energy of the states.

Table 4.1. Stark effect, perturbed and unperturbed energy differences E_{10} and E'_{10} for various dot size, infinitely deep potential, disc-like and spherical QD.

QD size parameter η	Disc-like QD $F = 10\ kV/cm$		Spherical QD $F = 10\ kV/cm$	
	E_{10} (eV)	E'_{10} (eV)	E_{10} (eV)	E'_{10} (eV)
8	0.126696582	0.126721105	0.146858175	0.146910031
10	0.081085813	0.081145565	0.093989232	0.094113221
12	0.056309592	0.056340568	0.065270331	0.065527553

Table 4.2. Stark effect, perturbed and unperturbed energy differences E_{10} and E'_{10} for various applied electric fields, infinitely deep potential, disc-like and spherical QD.

Applied Uniform Electric Field $F\ (kV/cm)$	Disc-like QD $\eta = 8$		Spherical QD $\eta = 8$	
	E_{10} (eV)	E'_{10} (eV)	E_{10} (eV)	E'_{10} (eV)
5	0.12669658	0.12670270	0.14685817	0.14687087
10	0.12669658	0.12672106	0.14685817	0.14691002
20	0.12669658	0.12679448	0.14685817	0.14706131

Table 4.3 presents the dipole matrix elements in the Stark effect case. As the field strrength increases, the diagonal elements increases. As a result, the nonlinear contribution of the second term in Equation (2.24) increases with the increasing field strength. On the other

hand, with increasing field strength, the off-diagonal perturbed dipole element μ'_{10} decreases.

Applied Uniform Electric Field $F\ (kV/cm)$	Disc-like QD $\eta = 8$		
	μ'_{10} (C.m.) x10^{-28}	μ'_{00} (C.m) x10^{-28}	μ'_{11} (C.m) x10^{-28}
5	1.98916	-0.156636	2.63251
10	1.97992	-0.313272	2.64256
20	1.94298	-0.626543	2.68276

Table 4.3. Stark effect, perturbed dipole matrix elements μ'_{00}, μ'_{11} and μ'_{10} for various applied electric fields, infinitely deep potential, disc-like QD.

The value of squared dipole matrix element $|\mu_{10}|^2$ plays important role in the optical susceptibilities, Equations (2.23) and (2.24). It is plotted as a function of QD size in Figure 4.6 for both the disc-like and spherical QDs. The confinement potential is infinitely deep potential.

The magnitude of the linear and the third-order nonlinear changes in the refractive index, $\Delta n^{(1)}$ and $\Delta n^{(3)}$, and of the linear and the third-order absorption coefficients, $\alpha^{(1)}$ and $\alpha^{(3)}$, depends on $|\mu_{10}|^2$. This squared value of the dipole element increases considerably with increasing QD size.

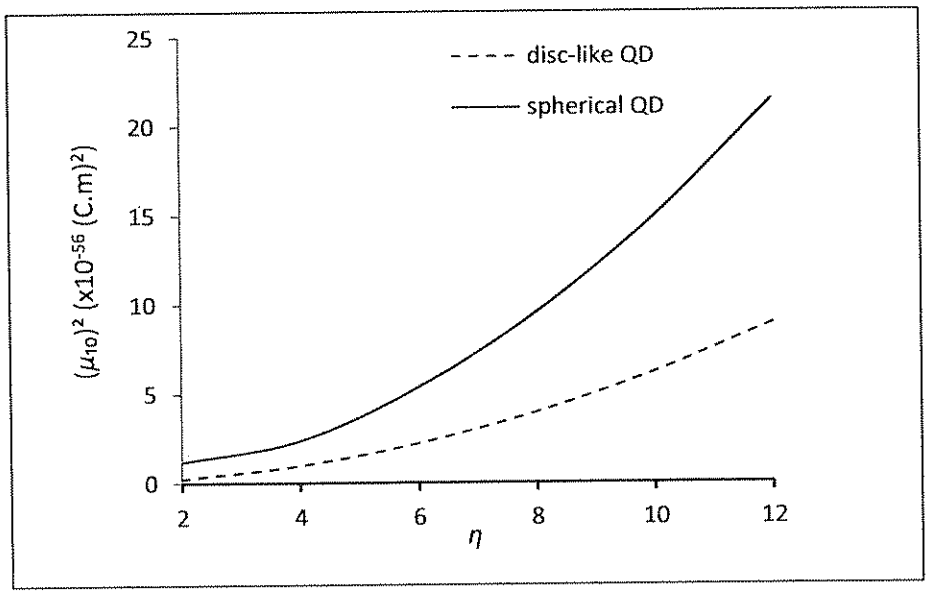

Figure 4.6. Effect of the QD shape on $|\mu_{10}|^2$, infinitely deep potential, no external field.

The difference in $|\mu_{10}|^2$ for the two different confinement potentials, infinitely deep and parabolic, in the disc-like QD can also be seen clearly in Figure 4.7. The dipole matrix elements between the ground and excited state is an increasing function of η, hence a decreasing function of ω_o.

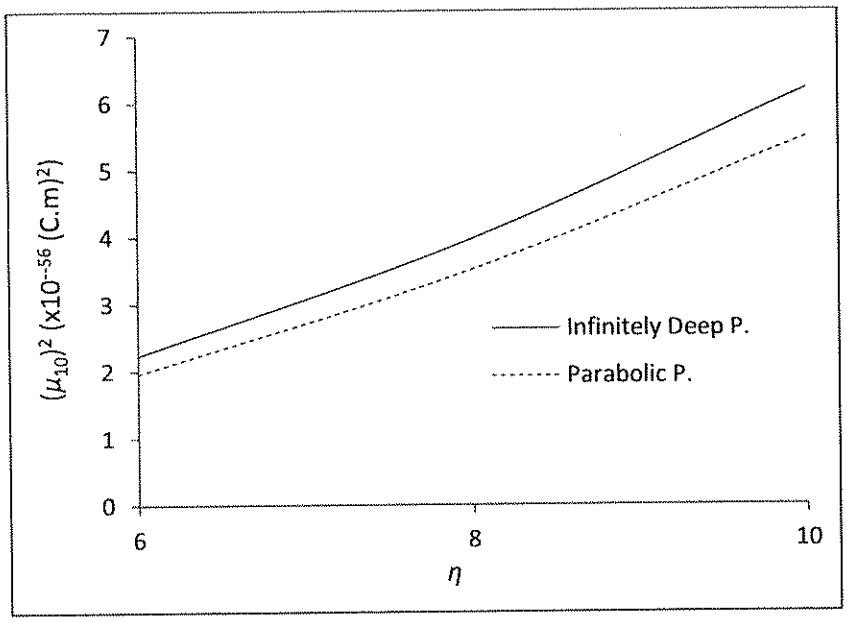

Figure 4.7. Effect of the confinement potential on the dipole matrix element $|\mu_{10}|^2$, disc-like QD, no external field.

The effect of the external uniform electric field, "Stark effect", Section 2.1.1. and 2.3.1, is also analyzed graphically. It is found that, for the spherical QD with infinitely deep potential, application of the external field does not change the symmetry of the potential, hence the refractive index changes and absorption coefficients stay almost same. The diagonal dipole matrix elements μ'_{00} and μ'_{11} are found to be exactly equal, therefore the second term in the third-order nonlinear susceptibility, Equation (2.24), and the change in ${\mu'_{10}}^2$ with the electric field is negligible.

But in the disc-like QD with infinitely deep confining potential, the changes in the dipole matrix elements and in the second term of the third-order nonlinear RIC are observed clearly. As the electric field strength F increases, $|\mu'_{10}|^2$ decreases, Figure 4.8, μ'_{00} is negative and its absolute value increases with increasing F and μ'_{11} is positive and increases with the field, Figure 4.9. In Figure 4.8, it is clearly seen that perturbed dipole matrix element $|\mu'_{10}|^2$ approaches to its unperturbed value $|\mu_{10}|^2$ when the field strength approaches to zero.

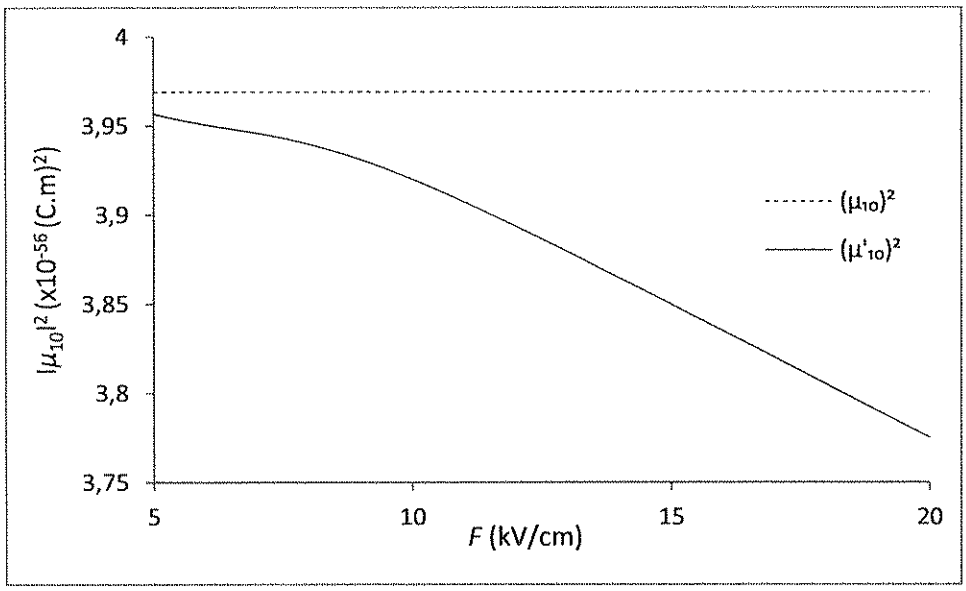

Figure 4.8. Effect of the external electric field F on the dipole element $|\mu_{10}|^2$, disc-like QD, infinitely deep potential, $\eta = 8$.

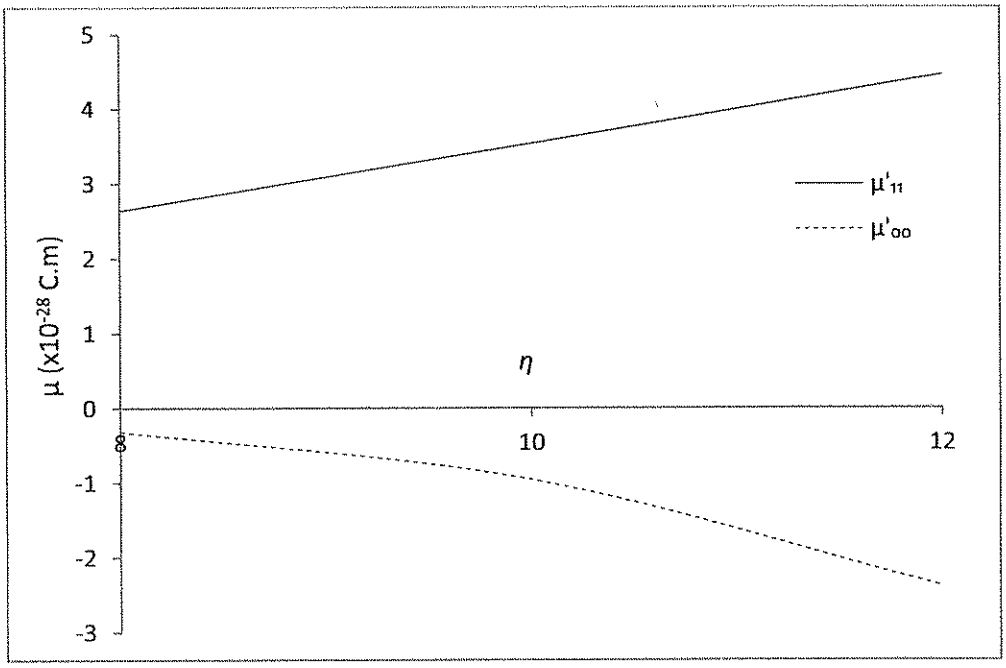

Figure 4.9. Variation of the diagonal matrix elements μ'_{00} and μ'_{11} with the size of disc-like QD, infinitely deep potential, $F = 10\ kV/cm$.

For different disc-like quantum dot sizes, the effect of electric field on the dipole element $|\mu_{10}|^2$ is shown in Figure 4.10. As the radius of the QD increases, the effect of uniform electric field increases.

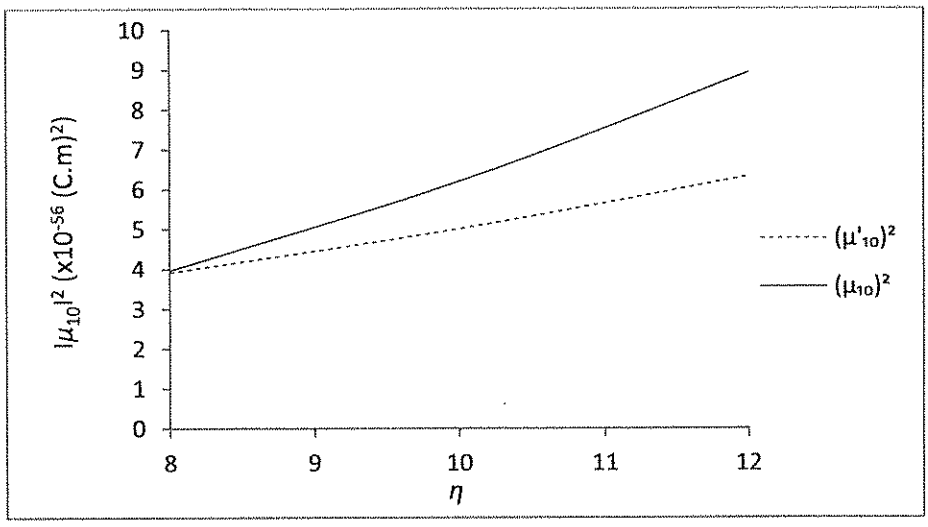

Figure 4.10. Effect of the external electric field F on the dipole element $|\mu_{10}|^2$, with different disc-like QD sizes, infinitely deep potential, $F = 10\ kV/cm$.

The coefficient of the second term, $|(\mu_{11} - \mu_{00})/\mu_{10}|^2$ in the third-order nonlinear susceptibility, Equation (2.24), is plotted in Figure 4.11. Increase of this term with increasing field strength F is clear. This indicates that the nonlinear contribution of the second term in Equation (2.24) increases as the strength of the external field increases.

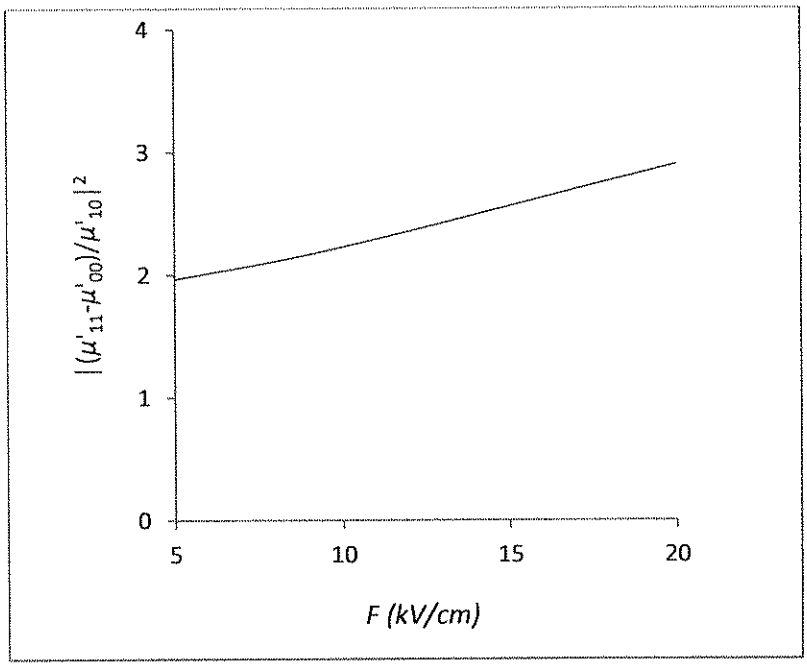

Figure 4.11 Variation of $|(\mu'_{11} - \mu'_{00})/\mu'_{10}|^2$ with the external electric field F, infinitely deep potential, disc-like QD, $\eta = 8$.

The diagonal dipole matrix elements μ_{00} and μ_{11} are zero when there is no external uniform electric field, but these elements are nonzero in "Stark effect" cases discussed in Section 4.1.1. and 4.3.1. The applied field disturbs the symmetry in the disc-like QD and the two states do not have a definite parity anymore.

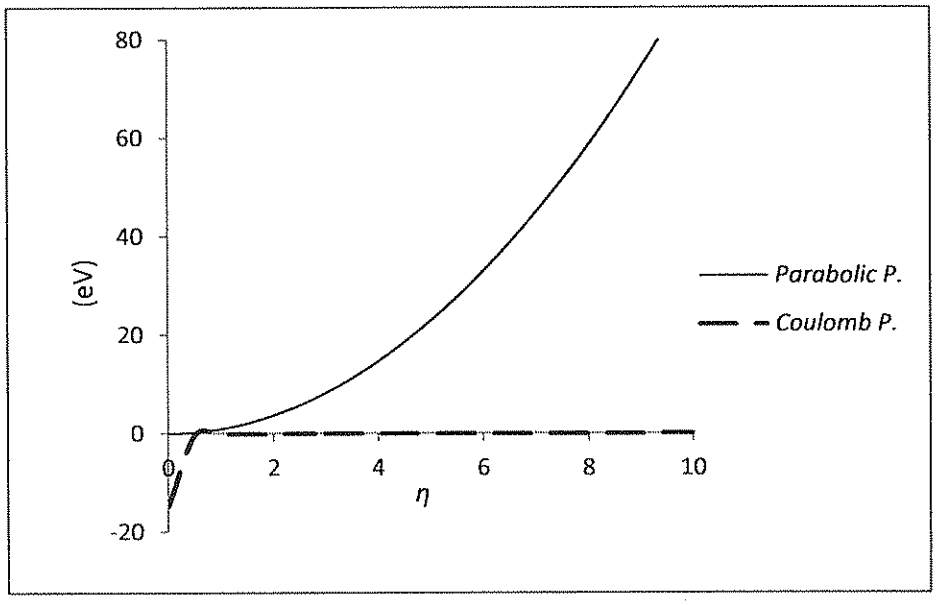

Figure 4.12. Variation of parabolic and Coulomb potential energies with QD size, disc-like QD, no external field.

In Figure 4.12, the parabolic potential energy (Equation (4.37)) and Coulomb potential $V(r) = -\mathrm{k}e^2/\in r$ are plotted for the disc-like QD. In this thesis, Coulomb interactions are neglected.

In Figure 4.13 the linear $\Delta n^{(1)}$, third-order nonlinear $\Delta n^{(3)}$ and total $\Delta n^{(total)}$ refractive index changes (RIC) are plotted as a function of the incident photon energy $h\nu$ for the disc-like QD with radius $a = 8a_o^*$. The intensity of the incident light is $I = 1.0\ MW/cm^2$ and the confinement potential is infinitely deep potential. There are two peaks at $E_{10} \pm \mathrm{i}\hbar\Gamma_o$, in each curve. One-photon resonance occurs when $h\nu = \hbar\omega \approx E_{10}$, it is $h\nu \approx 0.127\ eV$ for the disc-like QD with radius $a = 8a_o^*$.

The index of refraction n_r rises gradually with increasing frequency ω. However, in the vicinity of resonance, the index of refraction drops sharply, "anomalous dispersion". Between these two peaks, the absorption of the material reaches to maximum, the material may be opaque in this range [64]. $\Delta n^{(1)}$ is the largest contribution to the total refractive index change $\Delta n^{(total)}$.

The nonlinear RIC and the linear one generated by the $\chi^{(1)}$ term are opposite sign. Therefore, the total RIC will be obviously reduced if the nonlinear effect is considered. Thus, the nonlinear effects play an important role, and the calculation of RIC without the nonlinear term is not accurate enough.

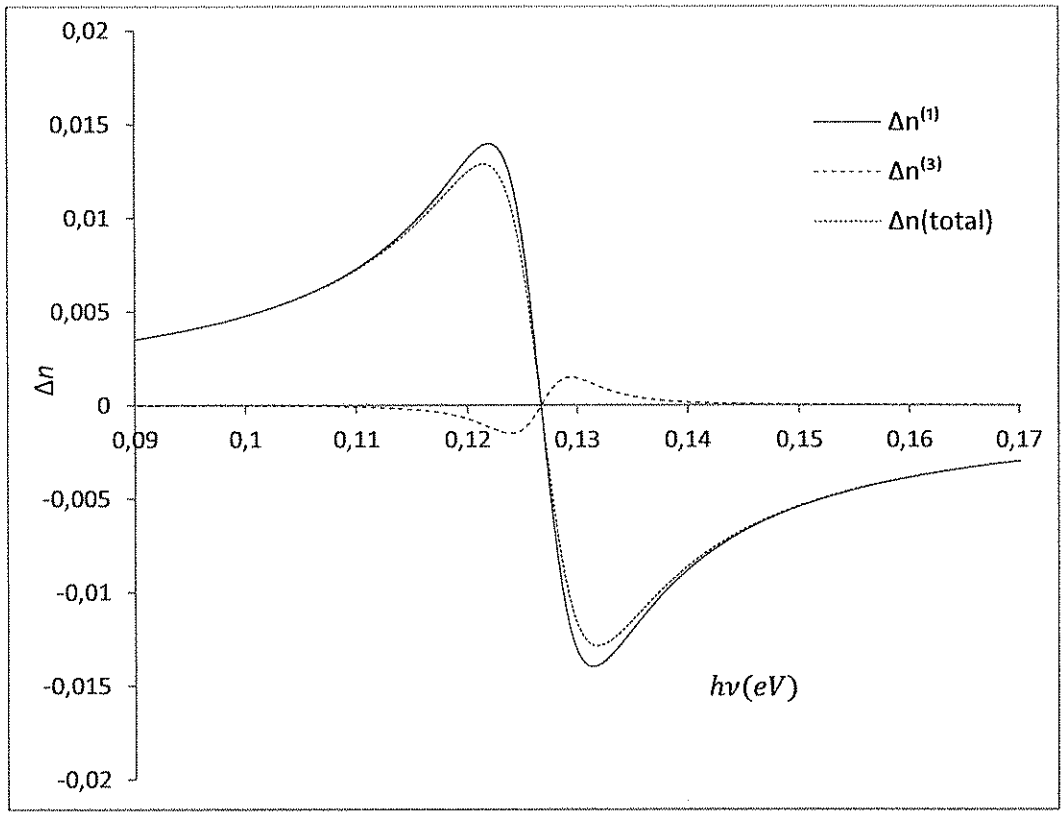

Figure 4.13. The linear, third-order nonlinear and total RIC as a function of photon energy, $\eta = 8$, $I = 1.0\ MW/cm^2$, disc-like QD, infinitely deep potential, no external field.

Linear, non-linear and total RIC as a function of the photon energy are also displayed for the disc-like QD in Figure 4.14, for various values of η which characterizes the QD size. The intensity of the incident light is $I = 1.0\ MW/cm^2$ and the confinement potential is infinitely deep potential. The peaks are blue-shifted for decreasing η. This is a result of increasing intersubband energy difference when the QD size becomes smaller, increasing the confinement effect. Since the linear change in the refraction index is related to the dipole matrix element $|\mu_{10}|^2$ which increases with the QD size ($a = \eta a_o^*$), the peaks in Figure 4.14 increase with η.

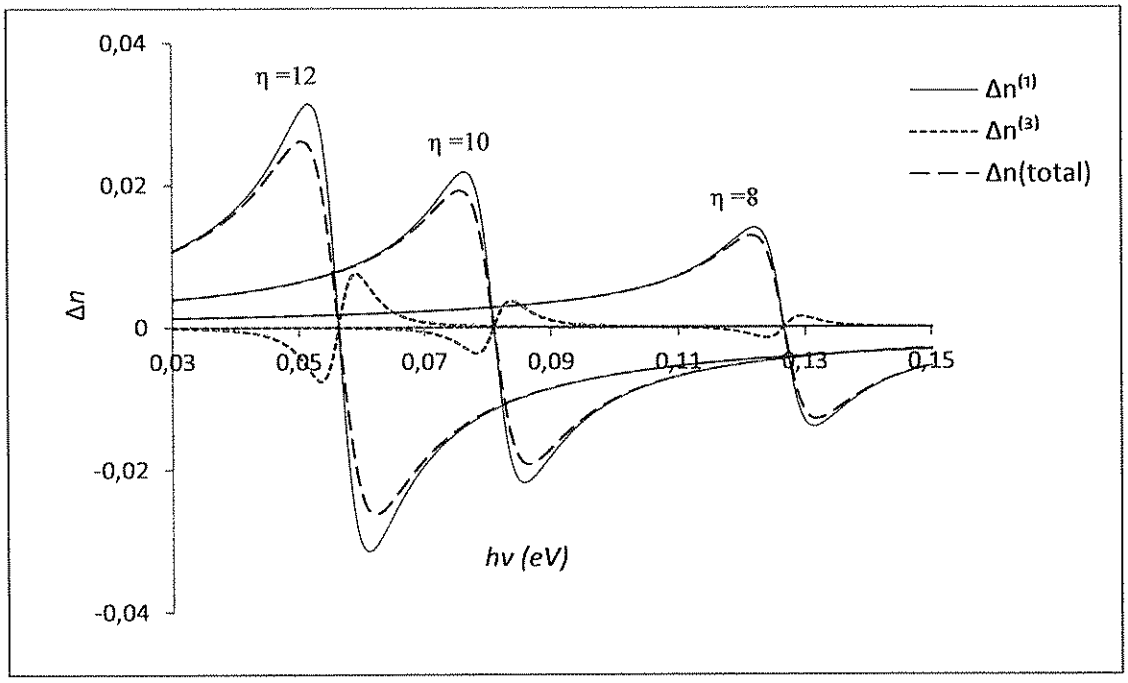

Figure 4.14. The linear, third-order nonlinear and total RIC as a function of photon energy, for various disc-like QD sizes, $I = 1.0\ MW/cm^2$, infinitely deep potential, no external field.

The changes in the third-order nonlinear refractive index $\Delta n^{(3)}$ and in the total refractive index $\Delta n^{(total)}$ as a function of photon energy for various intensities I, for the same value of $\eta = 8$, are given in Figure 4.15 and in Figure 4.16, respectively. The intensities are set to be $I = 0,\ 1.0, 1.5, 2.0\ MW/cm^2$. Infinitely deep potential is used. The total change in the index of refraction is reduced as the optical intensity is increased. This is a natural result of increasing negative contribution of nonlinear term which is directly proportional to the intensity. This nonlinear term has a large variation, and even may exceed the peak value of the linear refractive index change for high optical intensites. The sensitive dependence of $\Delta n^{(total)}$ to the shape and size of QDs, to the photon energy $h\nu$, to the optical intensity I and to the external fields makes this system ideal for nonlinear optical material applications One can control effectively the nonlinear response of the system [35,36].

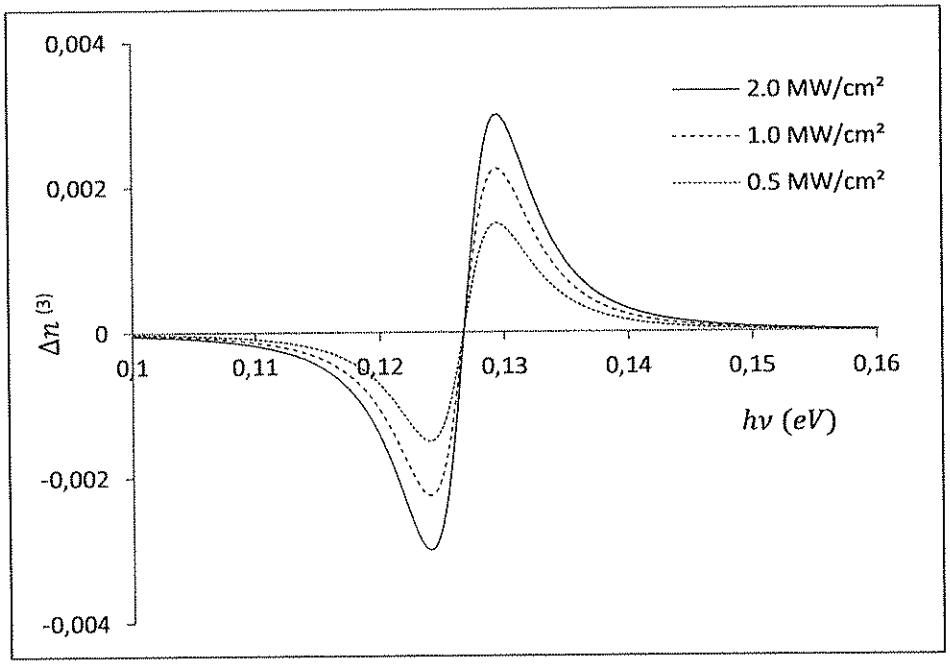

Figure 4.15. Third-order nonlinear RIC as a function of photon energy, for various intensities, $\eta = 8$, disc-like QD, infinitely deep potential, no external field.

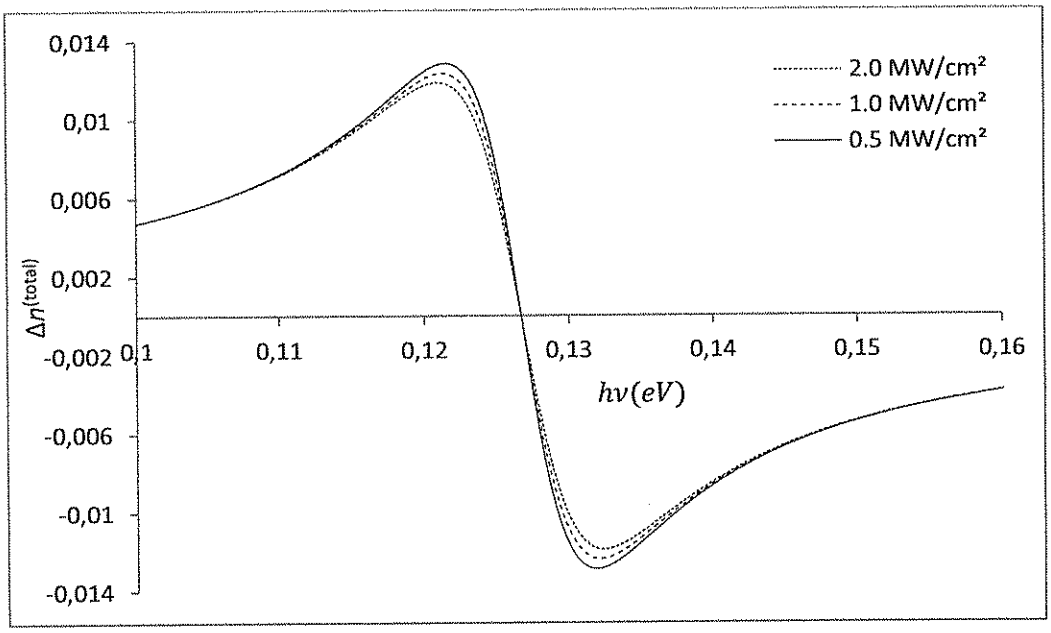

Figure 4.16. Total RIC as a function of photon energy, for various intensities, $\eta = 8$, disc-like QD, infinitely deep potential, no external field.

Linear, non-linear and total RIC as a function of the photon energy are plotted for the spherical QD in Figure 4.17, for various values of η. The intensity of the incident light is $I = 1.0\ MW/cm^2$ and the confinement potential is infinitely deep potential. As in the disc-like QD, the peaks are blue-shifted for decreasing η. The peaks are higher in the spherical QD case than those in the disc-like QD case. This is a result of increasing dipole matrix element $|\mu_{10}|^2$ which increases when the shape of the QD is spherical and with the QD size ($a = \eta a_o^*$). The peaks in Figure 4.17 increase with η.

One-photon resonance occurs when $h\nu \approx 0.146\ eV$ for the spherical QD of radius $a = 8a_o^*$. Since E_{10} is higher in the spherical dot, the resonance occurs at higher photon energies compared to the disc-like QD.

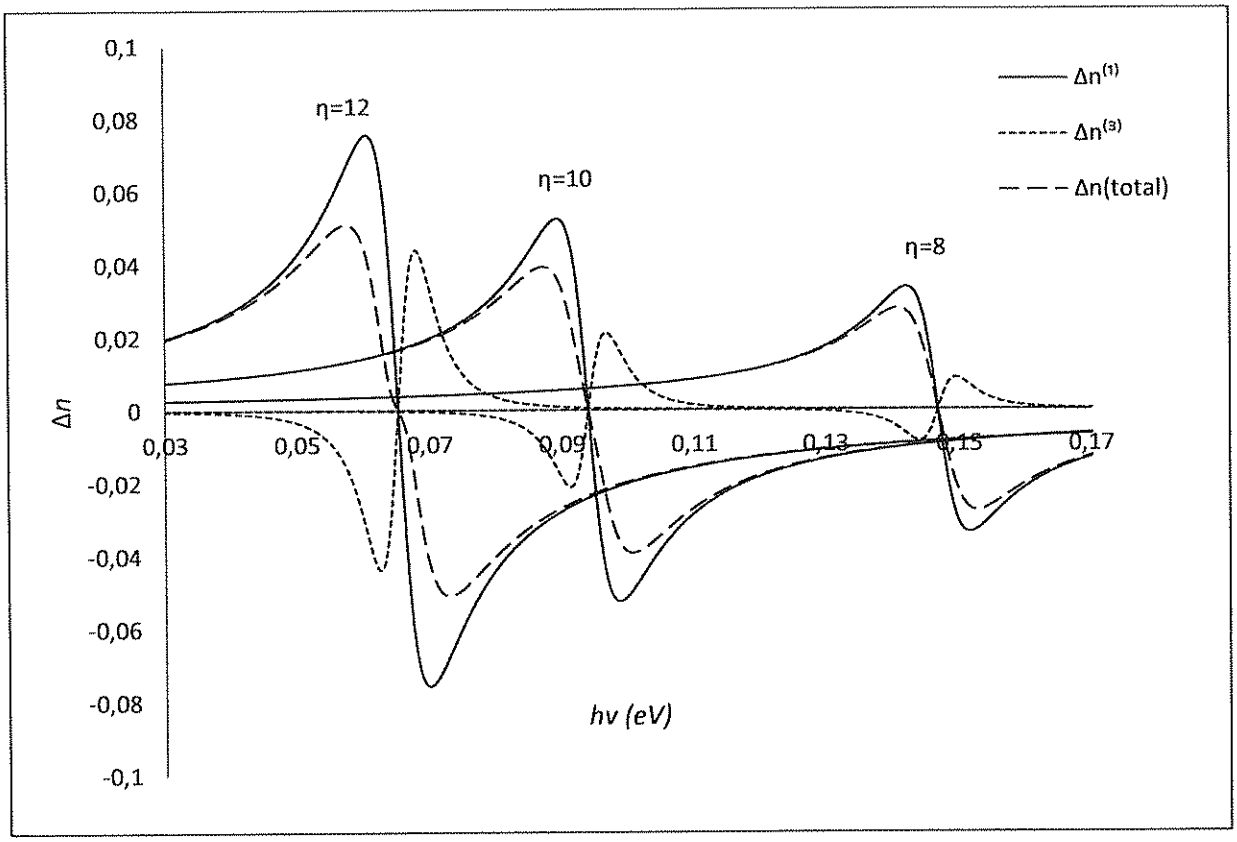

Figure 4.17. The linear, third-order nonlinear and total RIC as a function of photon energy, for various spherical QD sizes, $I = 1.0\ MW/cm^2$, infinitely deep potential, no external field.

$\Delta n^{(3)}$ and $\Delta n^{(total)}$ are shown as a function of photon energy for various intensities I, for the same value of $\eta = 8$, in Figure 4.18 and in Figure 4.19, respectively. The intensities are set to be $I = 0.5, 1.0,\ 2.0\ MW/cm^2$. Infinitely deep potential is taken.

Negative contribution of nonlinear term is bigger in the spherical case than that in the disc-like case, since $|\mu_{10}|^2$ is bigger in the disc-like QD. This term gets stronger with the increasing intensity, Figure 4.18. The effect of the intensity of the incident light on the RIC is more clear in the spherical case than that in the disc-like case.

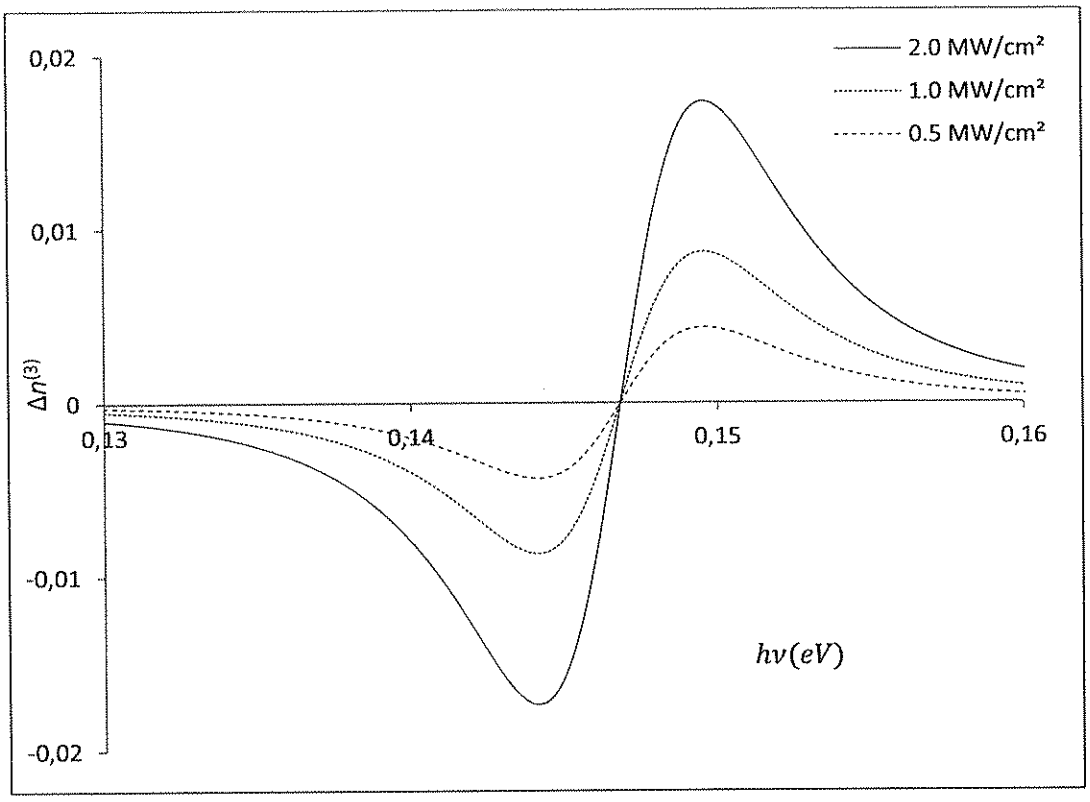

Figure 4.18. Third-order nonlinear RIC as a function of photon energy for various intensities, $\eta = 8$, spherical QD, infinitely deep potential, no external field.

The total RIC peaks decrease as the intensity increases as seen in Figure 4.19.

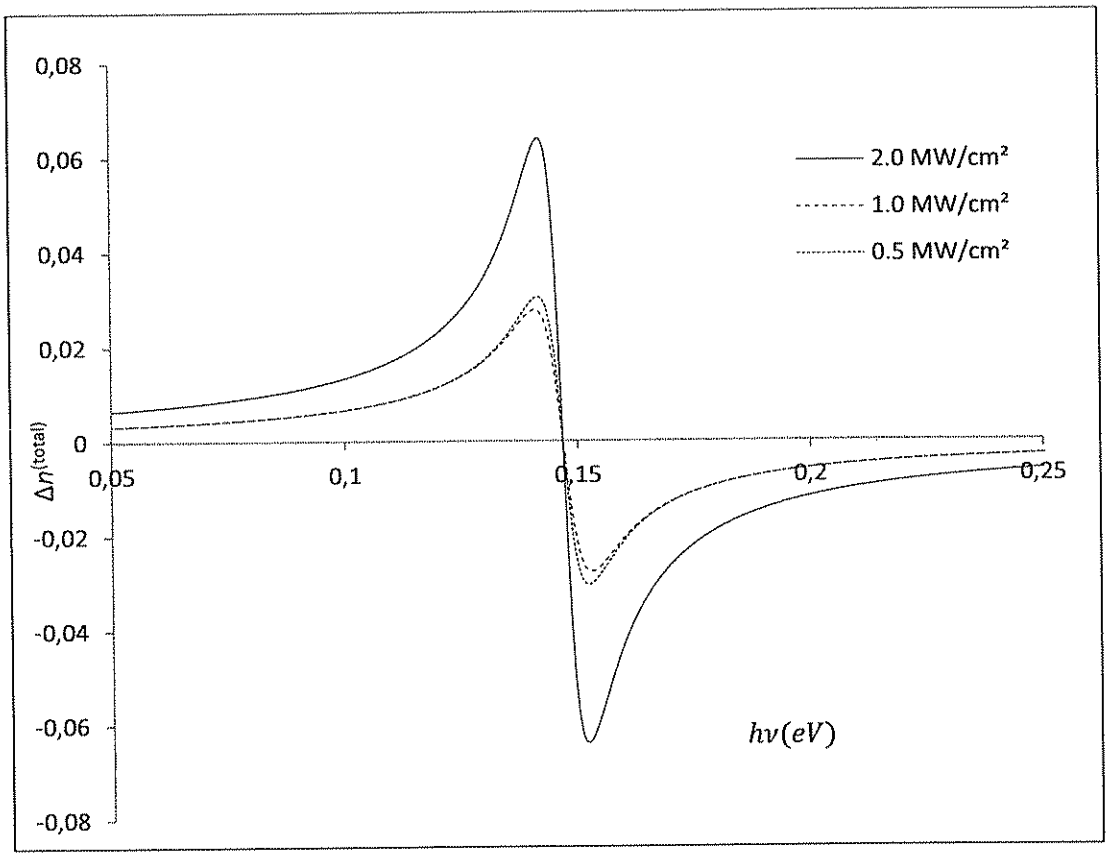

Figure 4.19. Total RIC as a function of photon energy for various intensities, $\eta = 8$, spherical QD, infinitely deep potential, no external field.

Figure 4.20 clearly presents the effect of the shape of QD on total RIC. For the same intensity and confining potential, the comparison shows that the optical response of the spherical QD is much stronger than that of the disc-like case.

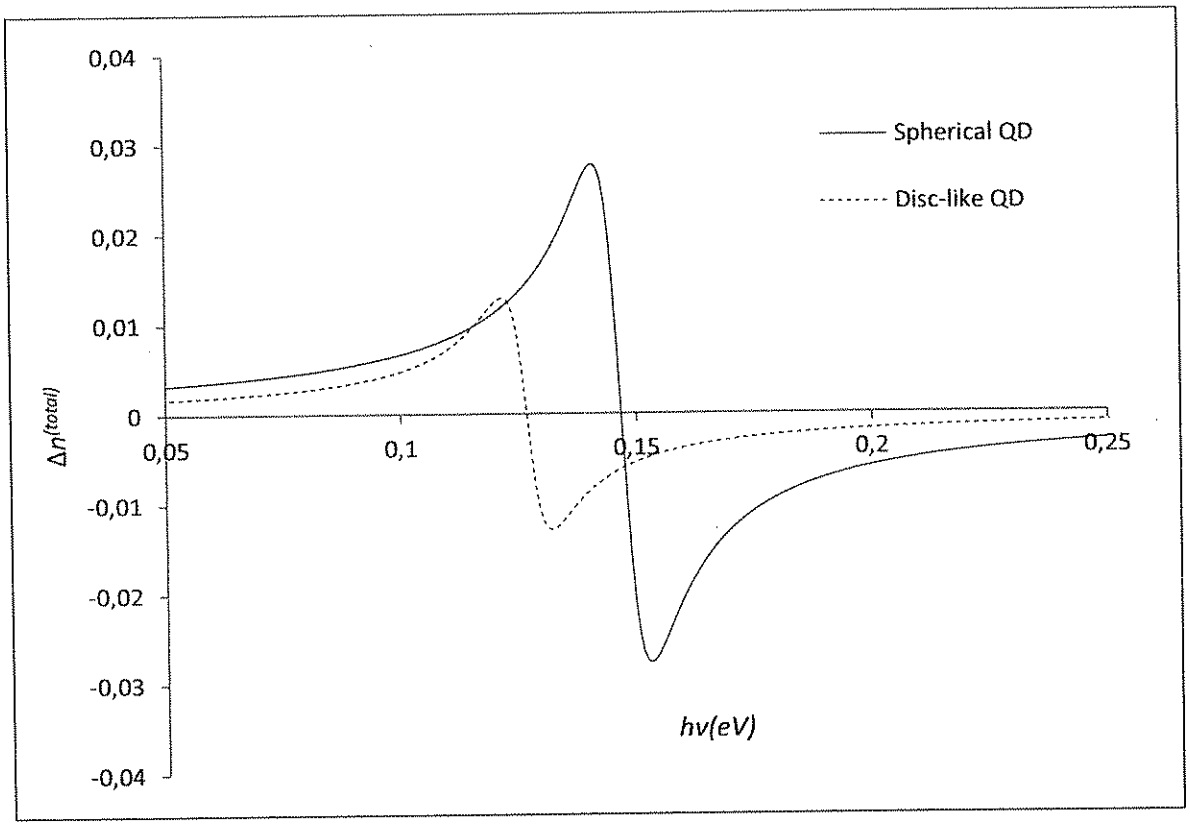

Figure 4.20. Comparison of total RIC of the spherical QD with that of the disc-like dot, infinitely deep potential, no external field, $I = 1.0\ MW/cm^2$ and $\eta = 8$.

The Stark effect on the disc-like QD is also analysed in Figure 4.21 and 4.22. Figure 4.21 and Figure 4.22 display the contribution of the second term in the Equation (2.24) to the change in the refractive index as a function of photon energy, for various disc-like QD size and external electric field strengths, respectively.

The asymmetry of the QD becomes stronger as the strength of the applied electric field increases. In this study, the maximum contribution of the second term in Equation (2.24) is determined at the incident photon energy $0.056eV$ in disc-like QD, with the electric field $F = 10\ kV/cm$ and $\eta = 12$. It is clear that the resulting nonlinearity is quite small. This is the reason why we find a rather small contribution to the change in the refractive index. The contribution is shown as a function of photon energy for various QD sizes in Figure 4.21 for the disc-like QD. With increasing dot size, the nonlinear contribution increases. The effect is found to be bigger for stronger electric fields.

The peak values are mostly negative and shift to higher energies for smaller QDs. This nonlinear term is not dominating the $\chi^{(3)}(\omega)$ values because of its small magnitude.

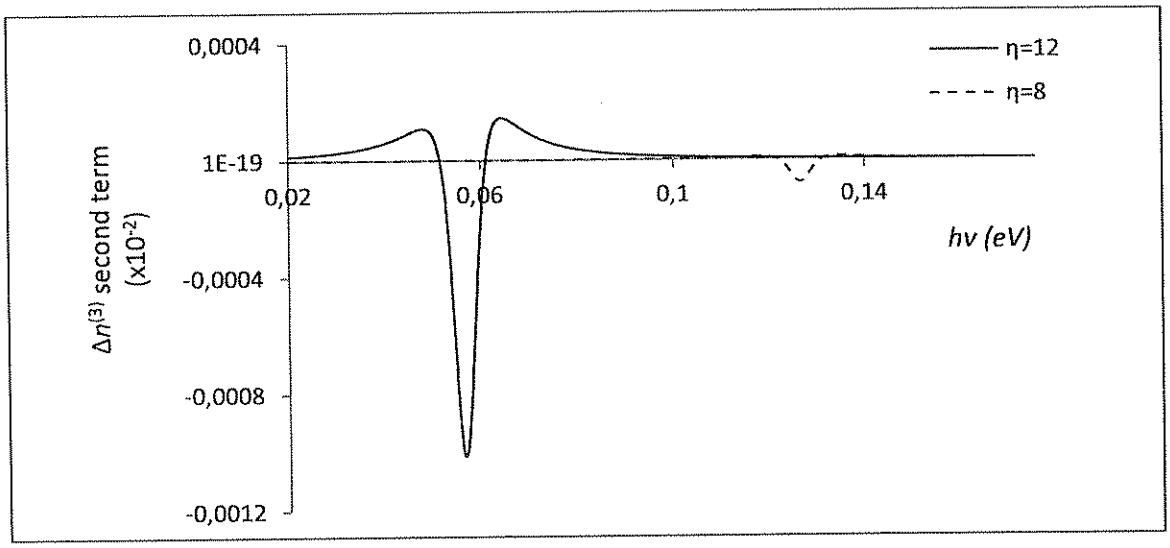

Figure 4.21. Contribution of the second term in Equation (2.24) to the change in the refractive index as a function of photon energy, for various disc-like QD size, infinitely deep potential, $F = 10\ kV/cm$, $I = 1.0\ MW/cm^2$.

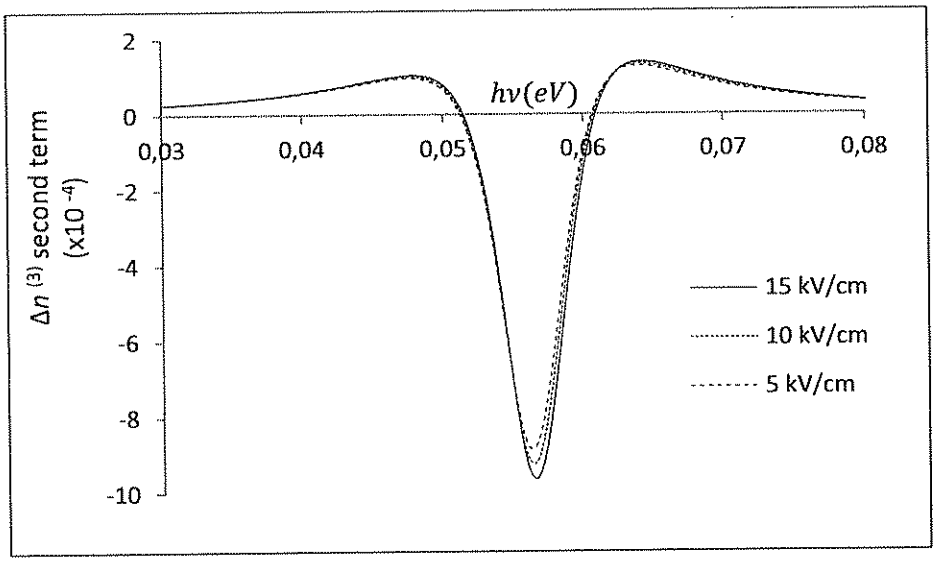

Figure 4.22. Contribution of the second term in Equation (2.24) to the change in the refractive index as a function of photon energy, for various external field strengths, disc-like QD, infinitely deep potential, $\eta = 8$, $I = 1.0\ MW/cm^2$.

In Figure 4.23, linear, non-linear and total RIC as a function of the photon energy are plotted for the parabolic potential case in the disc-like QD. There is no applied field F. As in the disc-like QD case with infinitely deep potential, the peaks are blue-shifted for decreasing η. The peaks are lower in the parabolic confinement than those obtained for the infinitely deep potential case. This is a result of decreased value of $|\mu_{10}|^2$ as shown Figure (4.7). One-photon resonance occurs when $h\nu \approx 0.146\ eV$ for the disc-like QD of radius $a = 8a_o^*$. Since E_{10} is lower (Figure 4.5) in the parabolic confinement, the resonance occurs at lower photon energies compared to the infinitely deep confining potential.

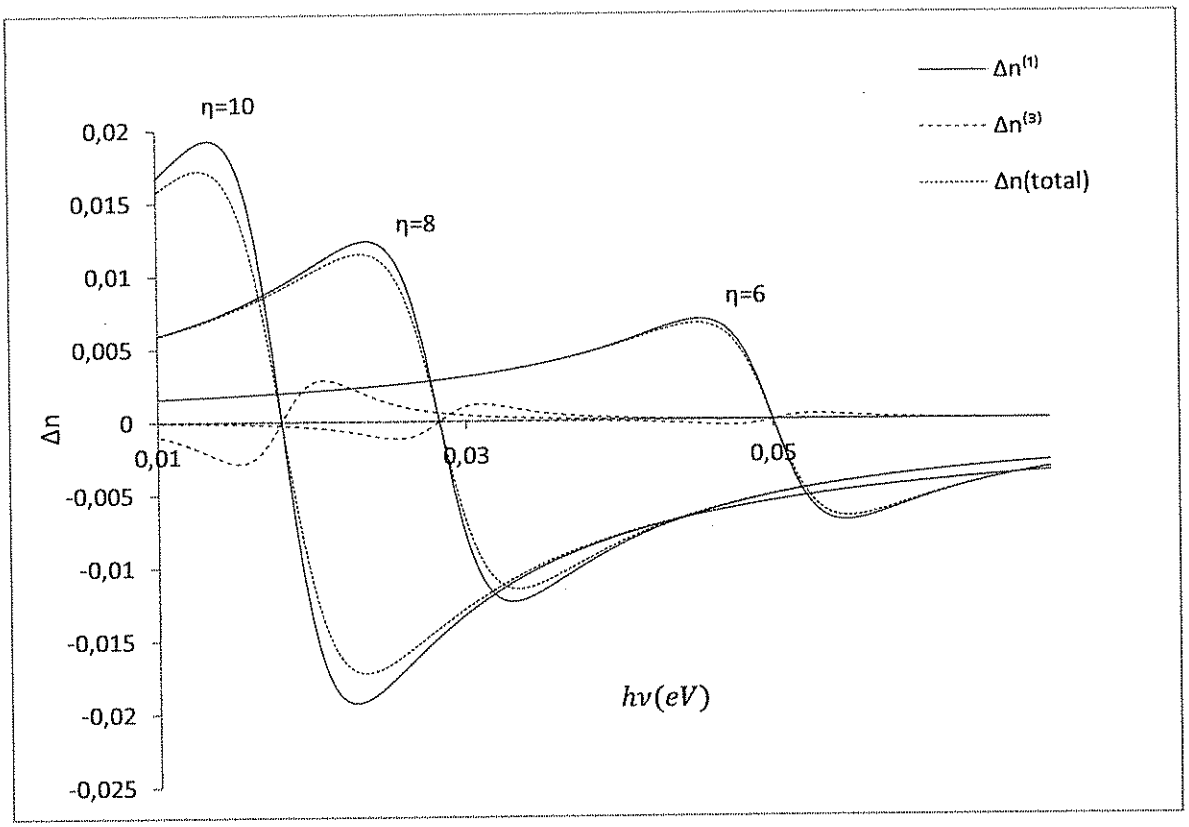

Figure 4.23. The linear, third-order nonlinear and total RIC as a function of photon energy, for various disc-like QD sizes, $I = 1.0\ MW/cm^2$, parabolic potential, no external field.

The effect of the confining potential on the total RIC is also illustrated in Figure 4.24 for the disc-like QD. The total RIC is plotted for the infinitely deep and parabolic confinements, for the same dot size and the intensity.

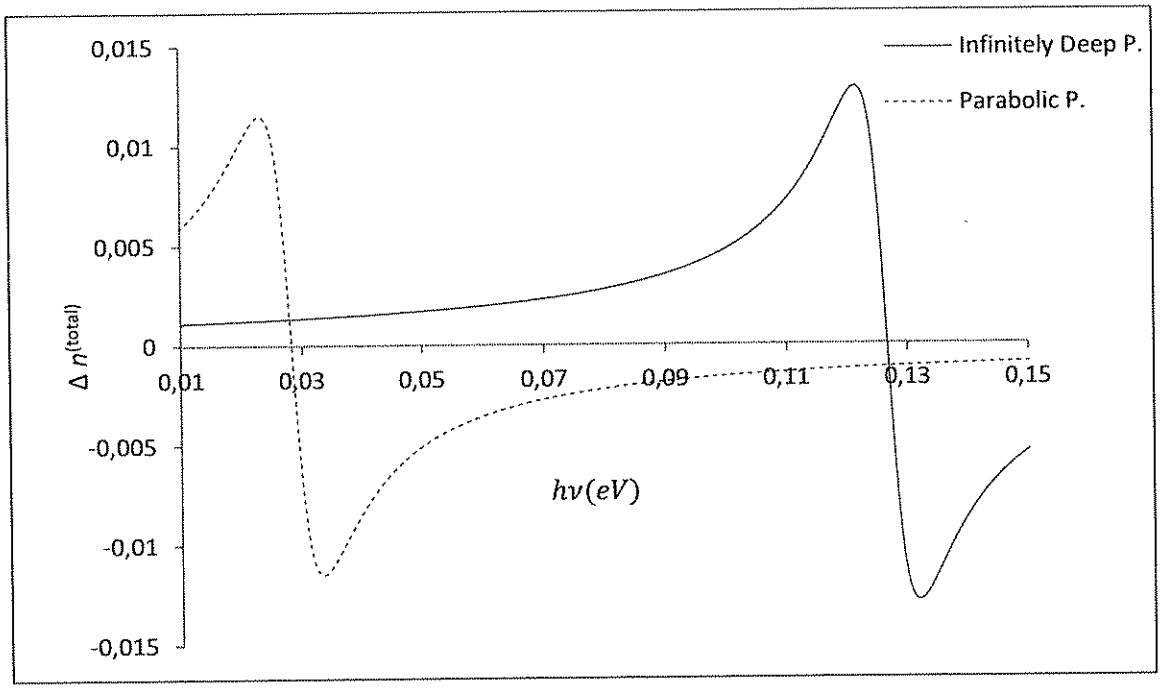

Figure 4.24. Effect of the confining potential on the total RIC in the disc-like QD, $I = 1.0\ MW/cm^2$ and $\eta = 8$, no external field.

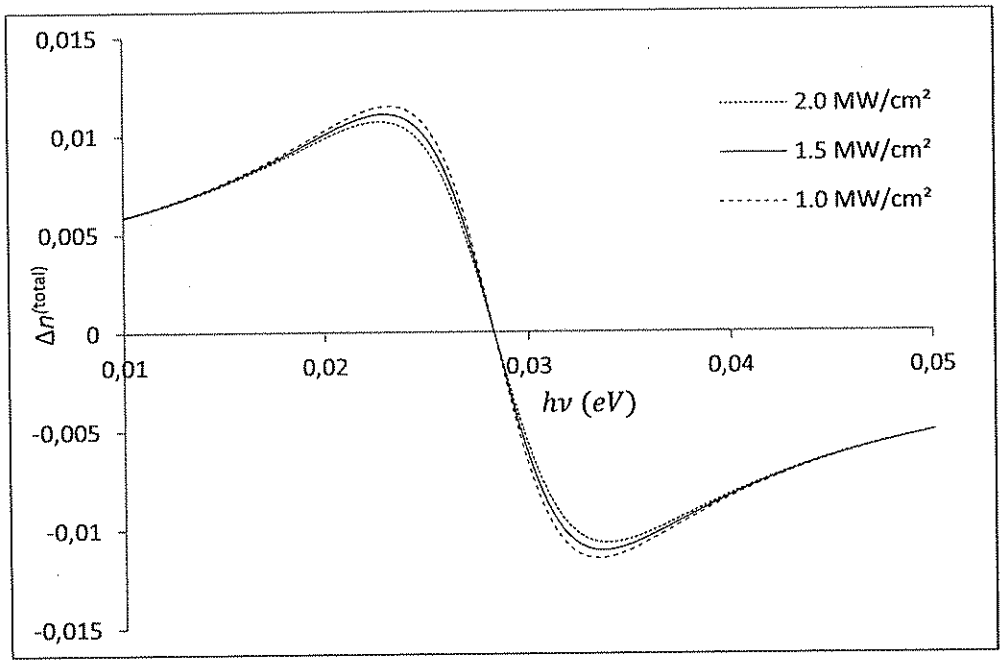

Figure 4.25. Total RIC as a function of photon energy for various intensities, $\eta = 8$, disc-like QD, parabolic confinement, no external field.

The intensity effect in the parabolic potential case is quite similar to that observed for the infinitely deep potential case in the disc-like QD. The nonlinear response increases as the intensity of the incident light increases. This is presented in Figure 4.25.

In Figure 4.26, the linear $\alpha^{(1)}$, third-order nonlinear $\alpha^{(3)}$and the total absorption coefficients $\alpha^{(total)}$ are illustrated as a function of incident photon energy, for the disc-like QD with infinitely deep confining potential. The intensity is taken as $I = 1.0\ MW/cm^2$. There is no external electric field. It is clear that the linear absorption coefficient $\alpha^{(1)}$ is large and positive while the nonlinear absorption coefficient $\alpha^{(3)}$ is smaller and negative. The plots indicate that the peaks are blue shifted with decreasing η.

The linear absorption coefficient $\alpha^{(1)}$ remains more or less constant but $\alpha^{(3)}$ decreases in negative height, i.e. , becomes more positive. This results in a slight increase in the total absorption coefficient. The total absorption coefficient increases with decreasing η. These results are obviously different from those of the RIC analysis of QDs. The nonlinear response of absorption increases strongly as the dot size decreases.

One-photon resonance occurs when $h\nu = \hbar\omega \approx E_{10}$, e.g. it is $h\nu \approx 0.127\ eV$ for the disc-like QD with radius $a = 8a_o^*$. At the resonance energies, the absorption peaks occur as seen in Figure 4.26 and the material may be opaque in that range of absorption graph, between the two positive and negative peaks of the refractive index change.

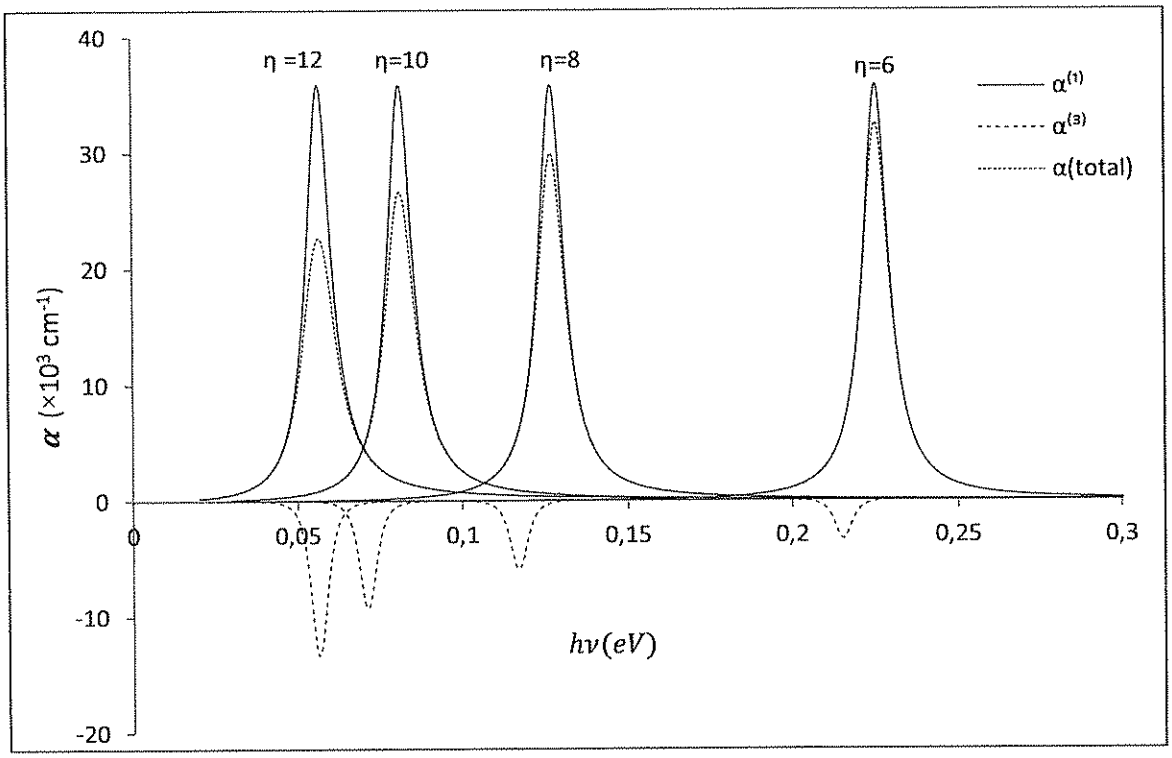

Figure 4.26. The linear, third-order nonlinear and total absorption coefficients as a function of photon energy, for various disc-like QD sizes, $I = 1.0\ MW/cm^2$, infinitely deep confining potential, no external field.

The absorption coefficients are also presented in Figure 4.27 for the spherical QD with infinitely deep confining potential. There is an absorption saturation at around $\eta = 12$ and $I = 1.0 \times 10^{10} W/m^2$, therefore it is not included. The absorption peaks have increased compared to those in the disc-like QD with the same potential. And they occur at higher photon energies. The increased peaks in spherical QD is due to the increased dipole matrix element $|\mu_{10}|^2$, hence the absorption coefficient is also directly related to the dipole matrix element $|\mu_{10}|^2$. This results can also be followed in Figure 4.28.

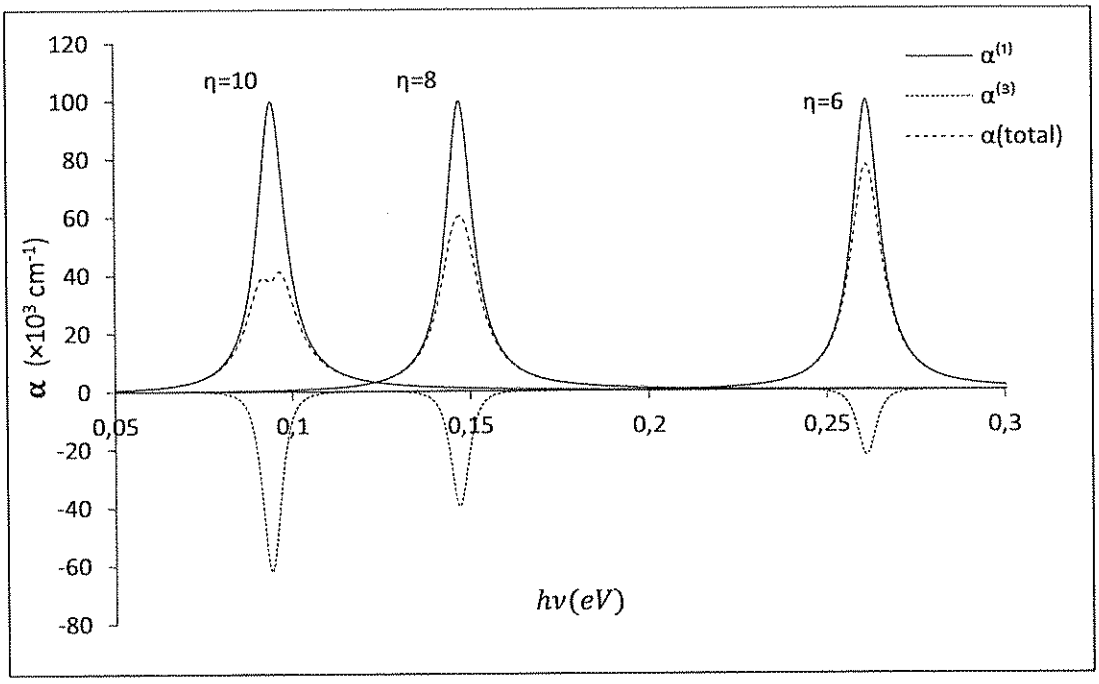

Figure 4.27. The linear, third-order nonlinear and total absorption coefficients as a function of photon energy, for various spherical QD sizes, $I = 1.0\ MW/cm^2$, infinitely deep confining potential, no external field.

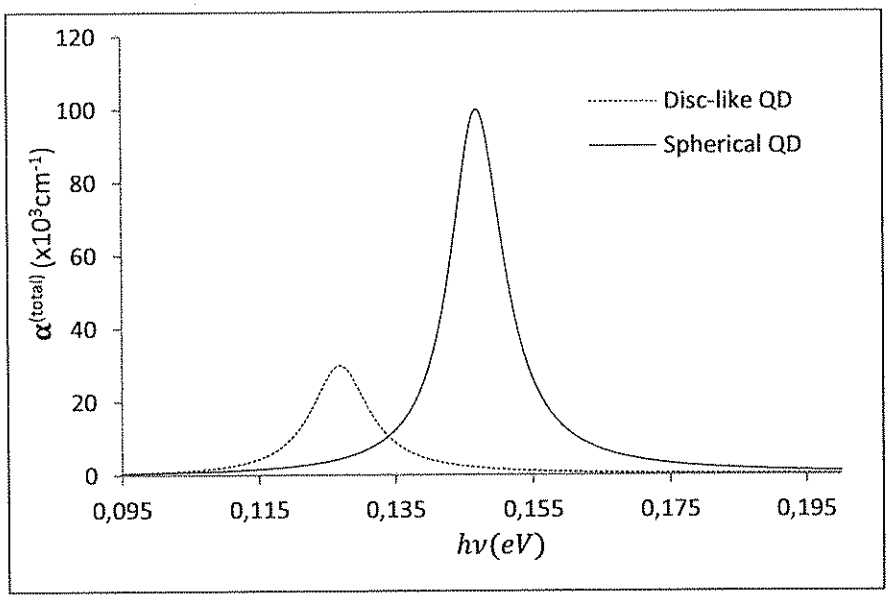

Figure 4.28. Effect of the QD shape on the total absorption coefficient $\alpha^{(total)}$, $\eta = 8$, $I = 1.0\ MW/cm^2$, infinitely deep confining potential, no external field.

The Figure 4.29 shows how the total absorption coefficient decreases with the parabolic confinement. The resonance peak also shifts to lower energies. The effect of the confining potential is also quite clear. The coefficients become larger with the infinitely deep potential compared to those with the parabolic confinement.

The blue shift of the peaks in the infinitely deep potential case is observed since this potential results in more localization. Its overall effect is equivalent to the effect of stronger confinement. So the presence of the infinitely deep confinement increases the absorption.

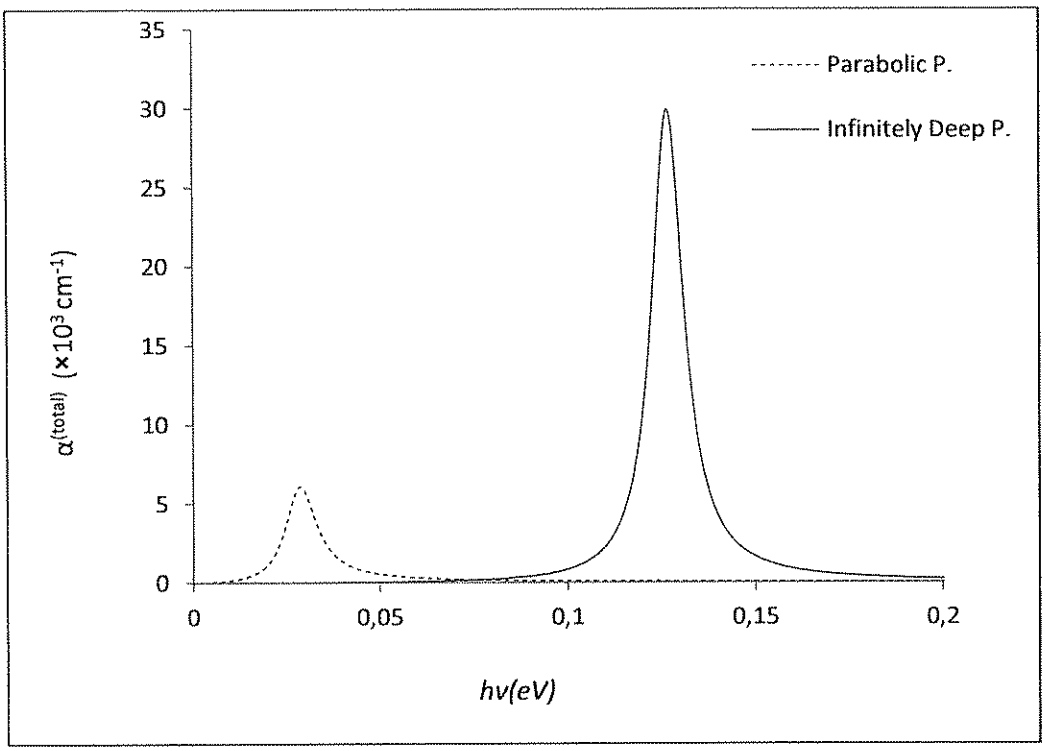

Figure 4.29. Effect of the confining potential on the total absorption coefficient $\alpha^{(total)}$, $\eta = 8,\ I = 1.0\ MW/cm^2$, infinitely deep confining potential, no external field.

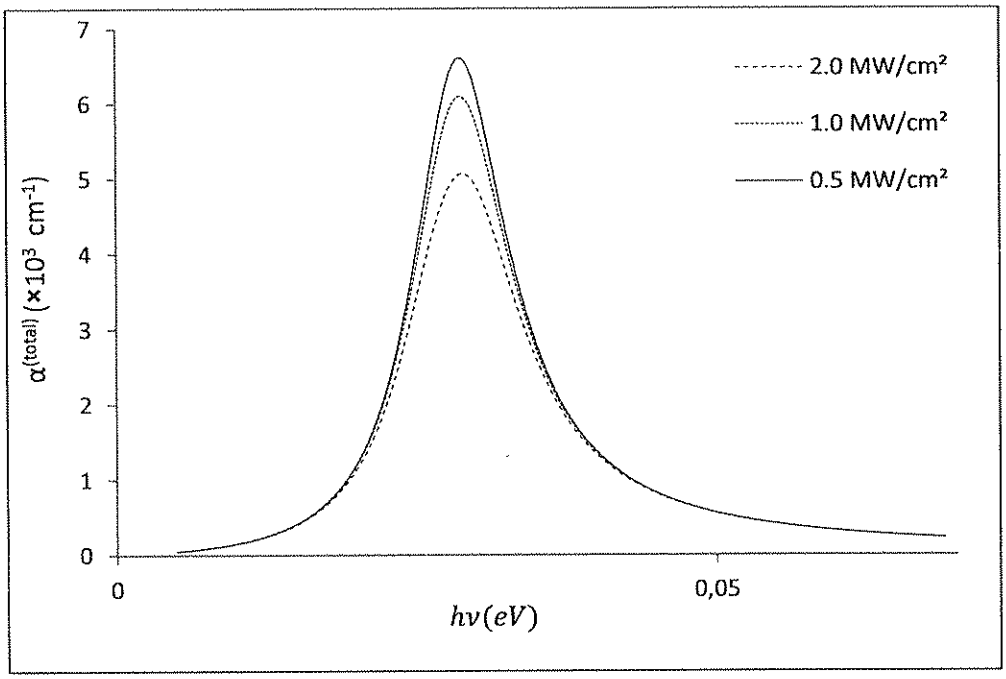

Figure 4.30. Effect of the intensity of the incoming photons on the total absorption coefficient $\alpha^{(\mathrm{total})}$, $\eta = 8$, disc-like QD, parabolic potential, $I = 1.0\ MW/cm^2$, no external field.

The effect of the intensity of the incoming photons is shown in Figure 4.30. The most important feature is that the total absorption coefficient becomes smaller as the intensity increases. At larger intensities the peak may develop into two peaks. It is for this reason we do not consider very large intensities.

The total absorption coefficient peak values for the disc-like QD are increasing with the parabolic confinement frequency ω_o. Thus the peaks are increasing with decreasing QD size. This is clearly shown in Figure 4.31, which presents $\alpha^{(\mathrm{max})}$ as a function of ω_o. The increase of frequency leads to an increase of intersubband energy difference and of the confinement effect, hence the absorption coefficient increases.

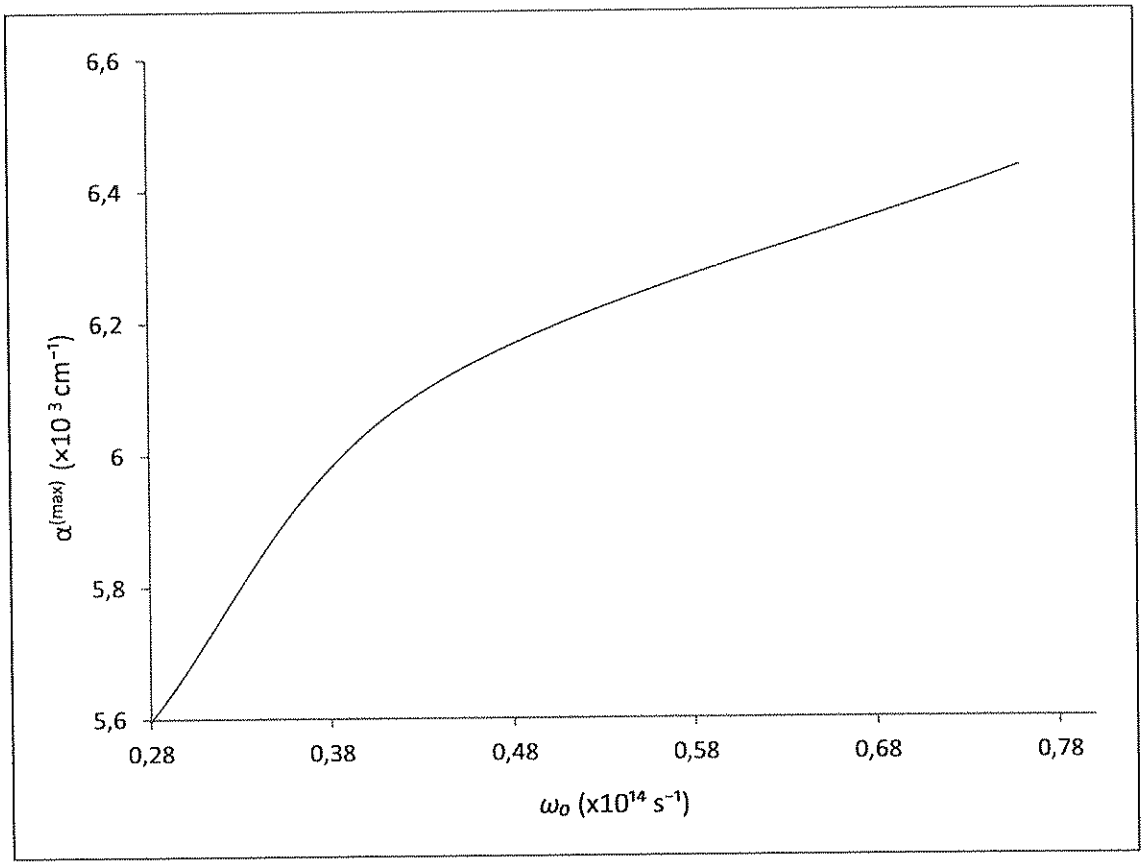

Figure 4.31. Variation of the maximum absorption coefficient $\alpha^{(max)}$ with the frequency ω_o of the parabolic potential, disc-like QD, parabolic potential, $I = 1.0\ MW/cm^2$, no external field.

5. CONCLUSION

In the present work, we have studied the changes in linear and third-order nonlinear refractive index and absorption coefficients for GaAs/AlGaAs QDs. Our results show that the changes in the refractive index and the optical absorption coefficients depend sensitively on the shape and size of the QDs and on the confinement potential.

Maximum changes in linear and nonlinear refractive index and maximum absorption coefficients are obtained in the spherical QD case compared to those obtained for the disc-like QD. The RIC peaks are blue-shifted for decreasing QD size. The total RIC will be obviously reduced if the nonlinear effect is considered. Thus, the nonlinear effects play an important role and the calculation of RIC and absorption coefficient without the nonlinear term is not accurate enough. The total absorption coefficient increases with decreasing QD size. This result is obviously different from that of the RIC analysis in QDs.

The RIC and absorption coefficients are larger with the infinitely deep confining potential, compared to those obtained with the parabolic potential. Infinitely deep confinement effects are stronger, hence the resultant optical response.

The nonlinear optical properties increase as the strength of the applied electric field and the optical intensity increase. One can engineer the structure of materials by means of external electric field and confinement strengths.

The results are in qualitative agreement with those in the literature.

REFERENCES

1. E. Rosencher and Ph. Bois., *Phys. Rev. B* 44(20), (1991) 11315-11327.

2. M. K. Gurnick and T. A. de Temple, *IEEE J. Quantum Electron.* QE 19, (1983) 791-794.

3. M. M. Fejer et al., *Phys. Rev. Lett.* 62, (1989) 1041-1044.

4. S. J. B. Yoo et al., *Appl. Phys. Lett.* 58, (1991) 1724-1726.

5. D. Walrod et al., *Appl. Phys. Lett.* 59, (1991) 2932-2934.

6. C. Lien, Y. Huang and J. Wong, *J. Appl. Phys.* 76 (1994) 1008-1012.

7. Y. Huang and C. Lien, *J. Appl. Phys.* 75 (1994) 3223-3225

8. A. Sa'ar et al., *Appl. Phys. Lett.* 61 (1992) 1263-1265.

9. F. Capasso, K. Mohammed and A. Y. Cho, *IEEE J. Quantum Electron.* QE-22 (1986) 1853-1869.

10. D.A.B. Miller, J.S. Weiner; DS Chemla, *IEEE J. Quantum Electron.* 22(9) (1986) 1816-1830.

11. P.F. Yuh and K.L. Wang, *Phys. Rev. B* 38(12) (1988) 8377-8382.

12. J. N. Heyman et al., *Phys. Rev. Lett.* 72 (1994) 2183-2186.

13. I. Karabulut, C. A. Duque, *Physica E-Low-dimensional Systems & Nanostructures* 43(7) (2011) 1405-1410.

14. G. H. Wang and K. X. Guo, *J. Condens. Matter* 13(35) (2001) 8197-8206.

15. G. H. Wang and K. X. Guo, *Physica B* 315(4) (2002) 234-239.

16. E. J. Roan and S. L. Chuang, *J. Appl. Phys.* 69(5) (1991) 3249-3260.

17. Y. B. Yu, S. N. Zhu, and K. X. Guo, *Solid State Commun.* 139 (2006) 76-79.

18. A. Hakimyfard, M.G. Barseghyan, A.A. Kirakosyan, *Physica E-Low-dimensional Systems & Nanostructures* 41 (2008) 1596-1599.

19. M. G. Barseghyan, A. Hakimyfard, S. Y. Lopez et al., *Physica E-Low-dimensional Systems & Nanostructures* 43 (2010) 529-533.

20. L. Tsang, D. Ahn, and S.L. Chuang, *Appl. Phys. Lett.*,52, 697 , (1998), 679-682.

21. R.Paiella, Intersubband Transitions in Quantum Structure, *McGraw-Hill* (2006)

22. B. Chen, K. X. Guo, R Z Wang, Y B Zheng, and B Li Chinese *J Physics* Vol. 47, N. 3(2009)

23. Y.Kayanuma *Physical Review B.* Vol.38, No.14, (1988)

24. S.V.Nair, S.Sinha, K.C.Rustagi, *Physical Review B.* Vol.35, No.8, (1986)

25. Ulrike Woggon, Optical Properties of Semiconductor QDs, *Springer,* Vol.136 (1958)

26. H.Haug, S.W.Koch, Quantum Theory of the Optical and Electronic Properties of Semiconductors, Fourth ed., *World Scientific* (2004)

27. L. Banyai, S.W. Koch, Semiconductor Quantum Dots, World Scientific, (1993)

28. P. Michler, Single Quantum Dots Fundamentalis , Applications and New Concepts.ed., *Springer,* (1963)

29. P. Y. Tong, *Solid State Commun.* 104, (1997), 679-682.

30. A. Harwitt and J. S. Harris, *Appl. Phys. Lett.* 50 (1987) 685-687.

31. S. Y. Yuen, *Appl. Phys. Lett.* 43 (1983) 813-815.

32. H. Yıldırım and M. Tomak, *Phys. Rev. B* (72) (2005) 115340 (1-6).

33. H. Yıldırım and M. Tomak, *J. Appl. Phys.* 99 (2006) 093103.

34. H. Yıldırım and M. Tomak, *Phys. Stat. Sol.* (b) 243 No:15 (2006) 4057-4063.

35. V. Ustoglu Unal, E. Aksahin, O. Aytekin, *Physics E*, 47, (2013), 103-108.

36. O. Aytekin, S. Turgut, V. Üstoğlu Ünal, E. Akşahin, M. Tomak, *Physica E*, 54, (2013), 257-261

37. B. A. Joyce, P. C. Kelires, A. G. Naumovets, D.D. Vvedensky, Quantum Dots: Fundamentals, Applications and Frontiers, *NATO* (2005)

38. D.A.B. Miller, *Int. J. High speed electron. Syst*, 1, (1991) 19.

39. B. Çakır, Y. Yakar and A. Özmen, *Progress in Electromagnetic Researches*, Vol.21 (2011) 77-92

40. W. Xie, *J. of Limunescense* 131 (2011) 943-946

41. İ.Karabulut, S. Baskoutas, *AIP Publising of Physics*, 103 (2008)

42. C. H. Liu, B. R. Xu, *Phys Lett. B* 372 (2008)

43. X. Xie, *Phys Scr.* 87 (2013)

44. X. Xie, S. Liang, *Physica B,* 406 (2011) 4657-4660

45. R.W. Boyd, Nonlinear Optics, third ed., *Academic Press, Elsevier,* San Diego, 2008.

46. J. J. Sakurai, Modern Quantum Mechanics, Rev ed., *Addison-Wesley, MA*, 1994.

47. J. B. Khurgin, *Phys Review B* (1988) 4056

48. D. Ahn and S.L. Chuang, IEEE J. Quantum Electron. QE-23 (1987) 2196-2204.

49. W. W. Bell, Special Functions for Scientists and Engineers, *Princeton.*

50. H. J. Arfken, G. B. Weber, Mathematical Methods for Physics, *Academic Press, Elsevier* (2005)

51. P. Harrison, Quantum Wells, Wires and Dots, Theoretical and Computational Physics of Semiconductor Nanostructures, Second ed., *Wiley-Interscience* (2005)

52. K.X. Guo and S. W. Gu , *Phys. Rev B,* 47, (1993) 16322.

53. P.F. Yuh and K.L. Wang, *J. Appl. Phys.* , 65, (1989) 4377.

54. L. Zhang and H.J. Xie, *Mod. Phys Lett. B*, 68, (2003) 235315.

55. L. Zhang and H.J. Xie, *Phys. Rev B*, 17, (2003) 347.

56. D. Ahn and S.L. Chuang, *IEEE J. Quantum Electron.* QE-23 (1987) 2196-2204.

57. J.C.M. Orozco, M.E. Mora-Ramos, C. A. Duque, *Physica Status Solidi* B249 (2012) 146-152.

58. J.C.M. Orozco, M.E. Mora-Ramos, C. A. Duque, *J. of Luminescence* 132 (2012) 449-456.

59. D. Ahn and S.L. Chuang, *J. Appl. Phys.* , 62(7), (1987) 3052-3055

60. R. W. Knoss, Quantum Dots: Research, Technology and Applications, *Nova* (2009)

61. P. Meystre, M.Sargent III, Elements of Quantum Optics, Fourth ed., *Springer* (2007)

62. P. Atkins, R. Friedman, Molecular Quantum Mechanics, *Oxford University Press*, Fourth ed. (2005)

63. R. J. Maygar, A Companion to Classical Electrodynamics, Third ed. (2001)

64. David J. Griffiths, Introduction of Quantum Mechanics, Prentice Hall